Electronic Supplementary Information

Minimizing the buried interfacial energy loss by a fluorine-substituted small molecule for 25.92%-efficiency and stable inverted perovskite solar cells

Xin Chen[a], Qi Wang[a], Wei Hui[b], Jiewei Yang[a], Yuqi Yao[a], Weijian Tang[c], Wuke Qiu[a], Xiaopeng Xu[a], Lin Song[b], Yihui Wu[a]*, and Qiang Peng[a]*

[a] School of Chemical Engineering, State Key Laboratory of Polymer Materials Engineering, Engineering Research Center of Alternative Energy Materials & Devices, Ministry of Education, Sichuan University, Chengdu 610065, P. R. China

[b] Frontiers Science Center for Flexible Electronics (FSCFE), Institute of Flexible Electronics (IFE), Northwestern Polytechnical University, Xi'an 710072, P. R. China

[c] College of Materials Science and Engineering, Sichuan University, Chengdu 610065, P. R. China

*E-mails: yihuiwu@scu.edu.cn, qiangpeng@scu.edu.cn

Materials

All the chemicals were used directly without further purification. Nickel oxide nanoparticle (99.999%), lead iodide (≥99.999%), formamidinium iodide (FAI, 99.9%), and C60 (99.5%) were purchased from Advanced Election Technology Co. Ltd. [2-(3,6-Dimethoxy-9H-carbazol-9-yl)ethyl]phosphonic acid (MeO-2PACz, >99%) was purchased from TCI. CsCl (99.999%), Tetrafluorosuccinic acid (TFSA, 97%), and 2,2-Difluorosuccinic acid (DFSA, 94%) were purchased from Alfa-Aesar. Succinic acid (SA, 99%) and anisole (>99.5%) were purchased from Aladdin. Methylammonium iodide (MAI, 99.9%) and 2,9-dimethyl-4,7-diphenyl-1,10-phenanthroline (BCP, 99%) was purchased from Xi'an Yuri Solar Co. Ltd. Dimethylformamide (DMF, 99.8%), dimethyl sulfoxide (DMSO, 99.9%), isopropyl alcohol (IPA, 99.5%) and Ethyl alcohol (EtOH, 99.5%) were purchased from Sigma-Aldrich. 1,3-Diaminopropane Dihydroiodide ($PDAI_2$, ≥99.5%) was purchased from Xi'an e-Light New Material Co, Ltd. Hydrogen peroxide (H_2O_2, ≥30%) was purchased from RESO.

Device fabrication

For the small size solar cell, FTO glass substrate was cleaned by sequentially washing with detergent, deionized water, acetone, and isopropanol (IPA). Before use, the FTO was cleaned with ultraviolet ozone for 15 min. Then, the substrate was spin-coated with a thin layer of NiOx nanoparticle (10 mg/mL aqueous solution containing 40 mol.% H_2O_2) at 2000 rpm for 40 s, and annealed in ambient air at 110 °C for 20 min, then cooled down naturally and transferred to glove box. 0.5 mg/mL MeO-2PACz was deposited on the NiOx at 3000 rpm for 25 s with annealed at 110 °C for 10 min. The buried interface passivators (SA, DFSA, and TFSA, 1 mg/mL in IPA) was capped on the MeO-2PACz layer at 5000 rpm for 25 s, and annealed at 110 °C for 10 min.

The RbCsFAMA-based perovskite solution was prepared by mixing 691.52 mg of PbI_2, 232.16 mg of FAI, 11.92 mg of MAI, 12.63 mg of CsCl and 9.56 mg of RbI in 1 mL of a mixed solvent (DMF:DMSO = 4:1, v/v), which was stirred for 12 h before use. The perovskite solution was filtered with 0.22 μm PTFE filter. After that, the perovskite ink was deposited on the FTO/NiOx/MeO-2PACz/passivator substrate by spin coating at 1000 rpm for 8 s with a ramp of 200, and 5000 rpm for 25 s (2000 rpm ramp). 20 seconds into the second step, 120 μL of

anisole was deposited onto the substrate. The wet film was then annealed at 110 ºC for 20 min. After that, 1 mg/ml $PDAI_2$ was coated on the perovskite surface at 4500 rpm for 25 s and annealed at 110 ºC for 5 min. Finally, 20 nm C_{60}, 6 nm BCP and 120 nm Ag were deposited by thermal evaporation.

The preparation method for CsFA-based (E_g=1.55 eV) and CsFAMA-based (E_g=1.55 eV) perovskite films were identical to that of RbCsFAMA-based perovskite film. The $Cs_{0.05}FA_{0.95}PbI_3$ perovskite precursor was prepared by dissolving 261.4 mg of FAI, 20.78 mg of CsI, 735.78 mg of PbI_2 and 22.26 mg of $PbCl_2$ in a mixed solvent solution (DMF: DMSO = 4:1, v/v, 1 mL) with a concentration of 1.6 M. The $Cs_{0.05}(FA_{0.95}MA_{0.05})_{0.95}PbI_3$ perovskite precursor solution was prepared by mixing 20.78 mg of CsI, 248.32 mg of FAI, 737.62 mg of PbI_2, and 12.08 mg of MAI in 1 mL DMF: DMSO (4:1 in volume) mixed solvent with a concentration of 1.6 M.

For the minimodule, a vacuum-assisted method was adopted to fabricate the large-area perovskite film. Briefly, the perovskite precursor was uniformly spread on the substrate with HTL and then spin-coated with a two-step process. The first step was 1000 rpm for 8 s with an acceleration of 200 rpm/s. The second step was 5000 rpm for 10 s with a ramp-up of 2000 rpm/s. The as-prepared wet perovskite film was put into a sample chamber which is connected with a pump system. Once valve was turned on, the solvent was removed rapidly under a low pressure maintained at 10 Pa for 10 s. After turning off the valve, the brown and transparent perovskite film is placed onto the hotplate. The perovskite films were annealed at 110 ºC for 60 min. All other processing technologies were kept the same as that of the small size perovskite device. A perovskite module with 6 series sub-cells was fabricated on an FTO glass substrate with a size of 5×5 cm^2. The series interconnection of modules was realized through P1, P2, and P3 lines. Pattern the lines using a laser scribing system with a wavelength of 1064 nm, a frequency of 20 KHz, a scan speed of 2000. For P1 line, a power of 16 W was used and the FTO substrate was scribed for 30 times. For P2 line, a power of 6 W was used, and the substrate was scribed for 1 time. For P3 line, a power of 10 W was used, and the substrate was scribed for 1 time. The widths of P1, P2 and P3 are 150, 500 and 100 μm, respectively. The width of each sub-cell was 6500 μm, while the width for a single dead area was 1100 μm. Therefore, the GFF was calculated to be 83.08%. After subtracting the dead area, the whole active area was calculated

to be 12.96 cm^2 for the minimodule (Fig. S27).

Characterization

X-ray Diffraction (XRD) patterns of the perovskite films were recorded on a Bruker D8 advance instrument equipped with Cu Kα radiation (40 kV, 40 mA). Scanning was performed at a rate of 5°/min in the 2θ range from 5-50° with a step size of 0.02 s. Grazing-incidence wide-angle X-ray scattering (GIWAXS) measurements were conducted at the BL14B1 beamline of Shanghai Synchrotron Radiation Facility (SSRF). The grazing incidence angle was 0.4°. The top-view, bottom-view, and cross-sectional SEM images were acquired using a Hitachi S4800 field-emission scanning electron microscopy system manufactured by Hitachi High Technologies Corporation. AFM measurements were conducted with a Bruker Innova atomic force microscopy. KPFM measurements were performed on a BRUKER ICON atomic force microscope under a PeakForce KPFM mode, and the scan rate was 0.5 Hz during the testing process. The samples were scanned in at least three random locations to ensure reliable results. Liquid state proton (^1H) and fluorine (^{19}F) nuclear magnetic resonance (NMR) measurements were recorded on a JNM-ECZ400S/L1 spectrometer using tetramethyl silane (TMS) as an internal standard (δ = 0). UV-vis absorption spectra of the solution and thin films were obtained using a PerkinElmer Lambda 950 UV-vis spectrophotometer without an integrating sphere. The scanning rate was set at 600 nm/min within the range of 900-200 nm, with a step bandwidth of 1 nm. The in-situ UV–vis absorption spectroscopy was recorded with Puguangweishi equipped deuterium light sources from 300 nm to 1100 nm in absorbance mode. The perovskite precursor solution was static spreading on the TFSA/FTO substrate, and it was spun at 1000 rpm for 8 seconds followed by 5000 rpm for 25 seconds. An antisolvent was dripped for the final five seconds before annealing on an in-situ UV-vis recorder at 110°C for 5 minutes to record its absorption behavior. Steady-state photoluminescence (PL) spectra and time-resolved PL decay measurements were carried out using an FLS980 Series Fluorescence Spectrometer. For PL measurement, excitation was provided by monochromatized Xe lamp emitting light at peak wavelength of 500 nm with line width of 2 nm. For TRPL, excitation source utilized supercontinuum pulsed laser sources (YSL SC-PRO) operating at an excitation wavelength of 800 nm and repetition rate of 0.1 MHz. Electrochemical impedance spectroscopy (EIS) was

conducted using a potentiometer (CHI604E, CH instrument) under dark conditions within the frequency range of 1 MHz to 10 MHz, with an AC amplitude of 5 mV. Mott-Schottky analysis was performed using a potentiometer (CHI604E, CH instrument) at a frequency of 1000 Hz and an applied voltage range from 0 V to 1.5 V, with an AC amplitude of 5 mV. Transient photovoltage (TPV) and transient photocurrent (TPC) signals were detected by Piaos 4.0 system (FLUXiM) with a 60 mW LED light source. Monochromatic external quantum efficiency (EQE) spectra were measured as functions of wavelength under alternating current mode utilizing monochromatic incident light intensity equivalent to 1×10^{16} photons cm^{-2} with bias voltage maintained at 0 V (QE-R3011). Light intensity emitted by solar simulator was calibrated against standard silicon solar cell provided by PV Measurements. The EQE of electroluminescence (EQE_{EL}) spectra of the PSCs were detected by ENLITECH REPS-VOC under dark conditions. *I-V* curves were performed at a test range of 0-1.5 V with a step length of 0.02, EL was measured at an applied voltage of 1.9 V, and then *I-V* and EL were fitted to obtain EQE_{EL}. Urbach energy was detected by HS-EQE (ENLITECH PECT-600) and obtained by fitting the tail of the band. Fourier transform infrared spectroscopy (FT-IR, Thermo Fisher Nicolet Is5) was utilized to collect FT-IR spectral data for samples without and with the treatments by functional molecules. UPS and XPS spectra were acquired using a Thermo-Fisher ESCALAB Xi+ system. For XPS measurement, radiation was generated by monochromatic excitation centered at 1486.7 eV from a 75 W Al Kα source. For UPS measurements, He I ultraviolet radiation source with energy of 21.22 eV was employed. Hall effect measurement was characterized by Lake shore Accent HL5500 Hall System. A magnetic field (B) (0-0.5 T) perpendicular to the sample surface was applied, and the test current range from -200 mA to 200 mA was applied using Keithley Model 2400. The samples were prepared by depositing perovskite film on glass substrate (1×1 cm^2), which contained two indium electrode (the distance between the two electrodes is 0.8 cm) depositing on the perovskite film for measurement. The current-voltage characteristics were measured using a Keithley 2400 source and solar simulator with standard AM1.5G illumination conditions (100 mW/cm^2, SAN EI: Japan), under ambient conditions.

The current-voltage characteristics were measured by Keithley 2400 source and the solar simulator with standard AM 1.5G (100 mW/cm^2, SAN EI: Japan) under ambient conditions. The light intensity was calibrated by a Newport-calibrated standard silicon solar cell. The *J-V*

curves were measured by forward (-0.1 V to 1.5 V forward bias) or reverse (1.5 V to -0.1 V) scans with a voltage step of 20 mV and a delay time of 100 ms for each point. The active area of a PSC was 0.12 cm^2. The *J-V* curves for all small sized devices were obtained by masking the cell with a metal mask of 0.09 cm^2 in area. Devices for long-term stability assessment were stored in an N_2-filled glovebox. After various time intervals, *J-V* measurements were conducted. The thermal stability of devices was measured regularly after heating on 85 ºC. The dynamic maximum power point (MPP) tracking was conducted within a custom-built N_2-filled enclosure under continuous 1 sun illumination using a white light LED array, while maintaining a temperature of approximately 30 ± 5 ºC (Multi-Channels Solar Cells Stability Test System, Wuhan 91PVKSolar Technology Co. Ltd, China). The MPP was automatically recalculated every 2 hours by continuously monitoring the *J-V* curve.

The surface tension was obtained by a surface tensiometer (Germany, dataphysics, DCAT25) and calculated it further to acquire the Flory-Huggins interaction parameter (χ). The surface tension of each molecule was obtained by measuring the contact angles of MeO-2PACz, SA and their fluorine-containing derivatives to water and diiodomethane, respectively. Finally, the Flory-Huggins interaction parameter (χ) of MeO-2PACz/SA, MeO-2PACz/DFSA, and MO-2PACz/TFSA were obtained by the following equation:

$$\chi = k(\sqrt{\gamma_{MeO-2PACz}} - \sqrt{\gamma_{buried\ passivators}})^2$$

Where, the $\gamma_{MeO\text{-}2PACz}$, and the $\gamma_{buried\ passivators}$ are the surface energy of MeO-2PACz and buried interface passivators (SA, DFSA, and TFSA), respectively.

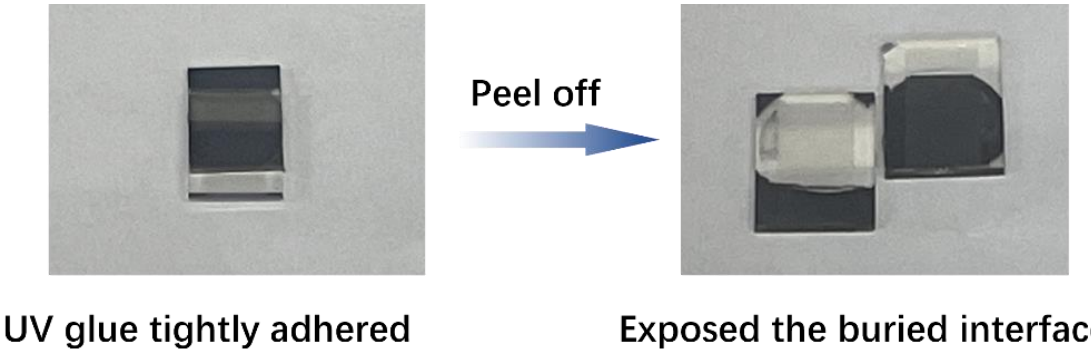

Fig.S1. The illustration of the fabrication process for exposing the buried interface of perovskite.

The perovskite films exposed the buried surface were fabricated according to the reported literature.[1] Briefly, the as prepared perovskite films were rinsed by utilizing a mixed solvent (IPA: DMF=150: 1, v/v) at 5000 rpm for 25 seconds. Then, a small amount of UV curable glue was dropped onto a clean glass substrate, and then the substrate was covered onto the upper surface of the perovskite films based on different substrates. After that, the substrate is pressed to closely contact the perovskite. Then, ultraviolet light was used to solidify the glue. Finally, perovskite film was mechanically peeled off and completely transferred to the substrate.

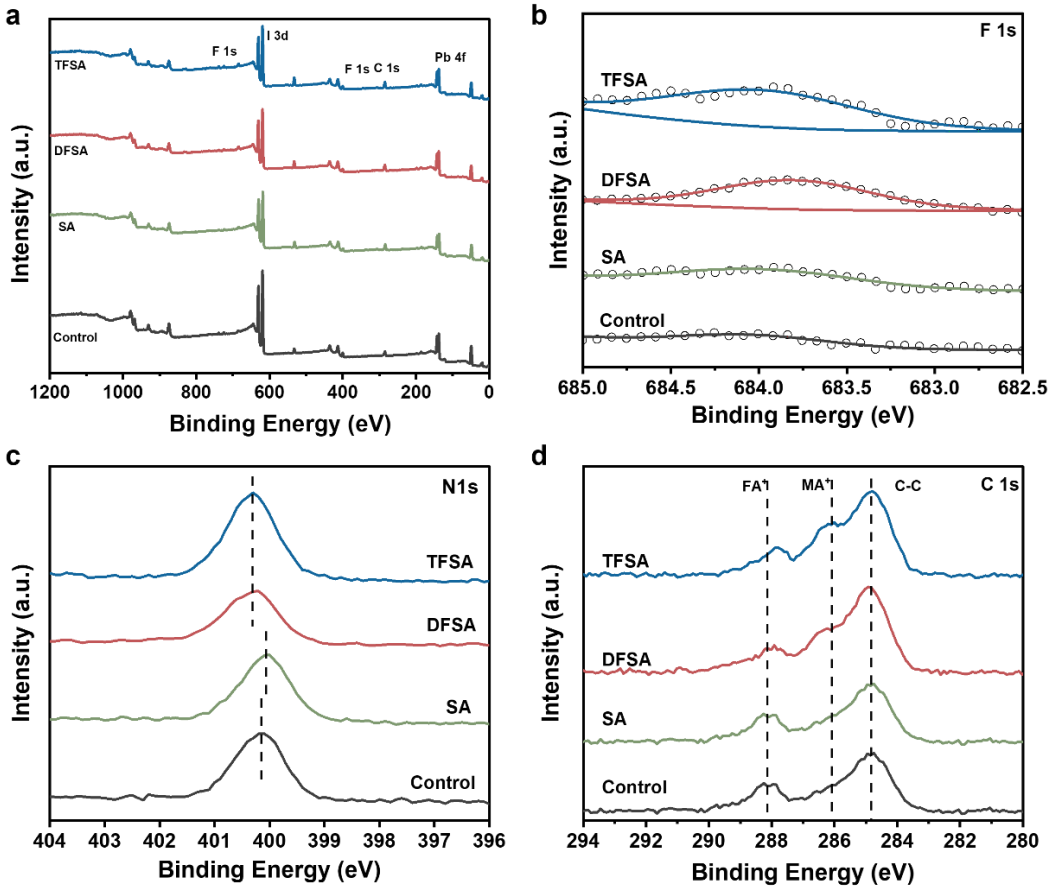

Fig. S2. XPS spectra of perovskite films exposed the buried surface without and with the treatment of SA derivatives. (a) The survey, (b) F 1s signals, (c) N 1s signals, and (d) C 1s.

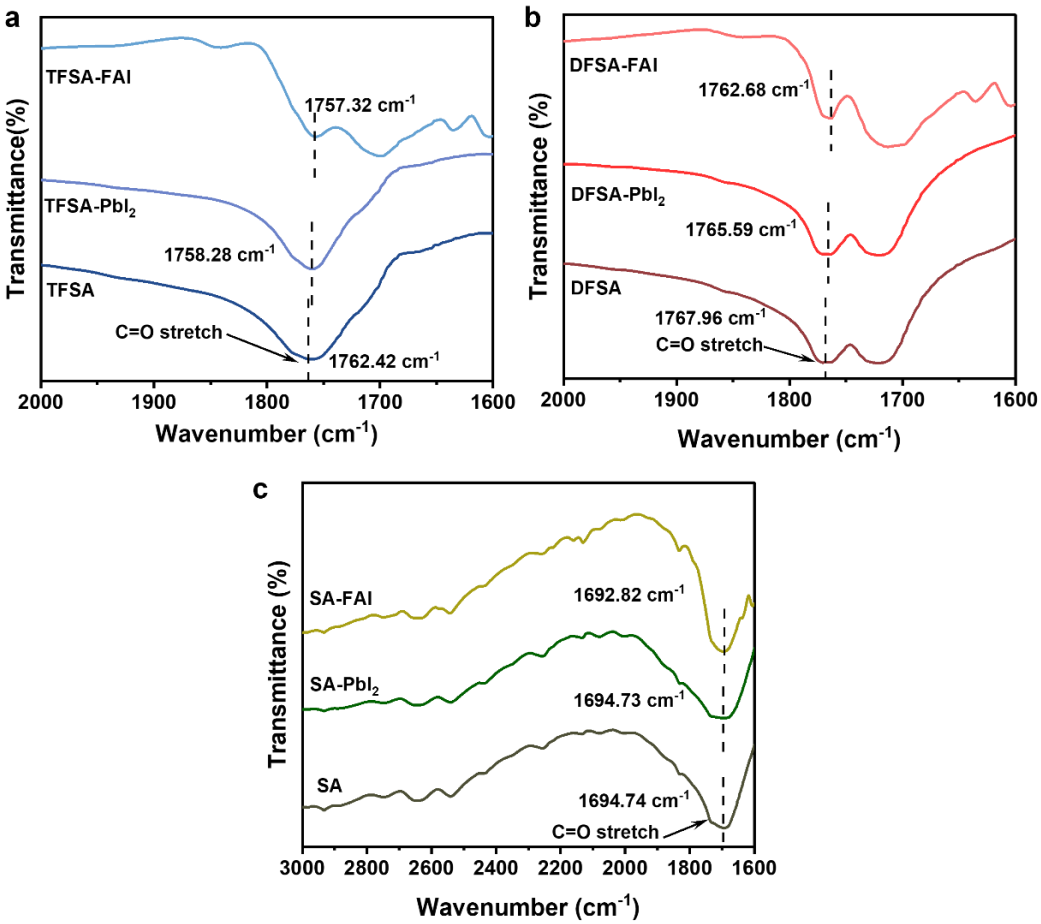

Fig. S3. Partial enlarged FT-IR spectra of (a) TFSA, TFSA-PbI_2 and TFSA-FAI, (b) DFSA, DFSA-PbI_2 and DFSA-FAI, (c) SA, SA-PbI_2 and SA-FAI.

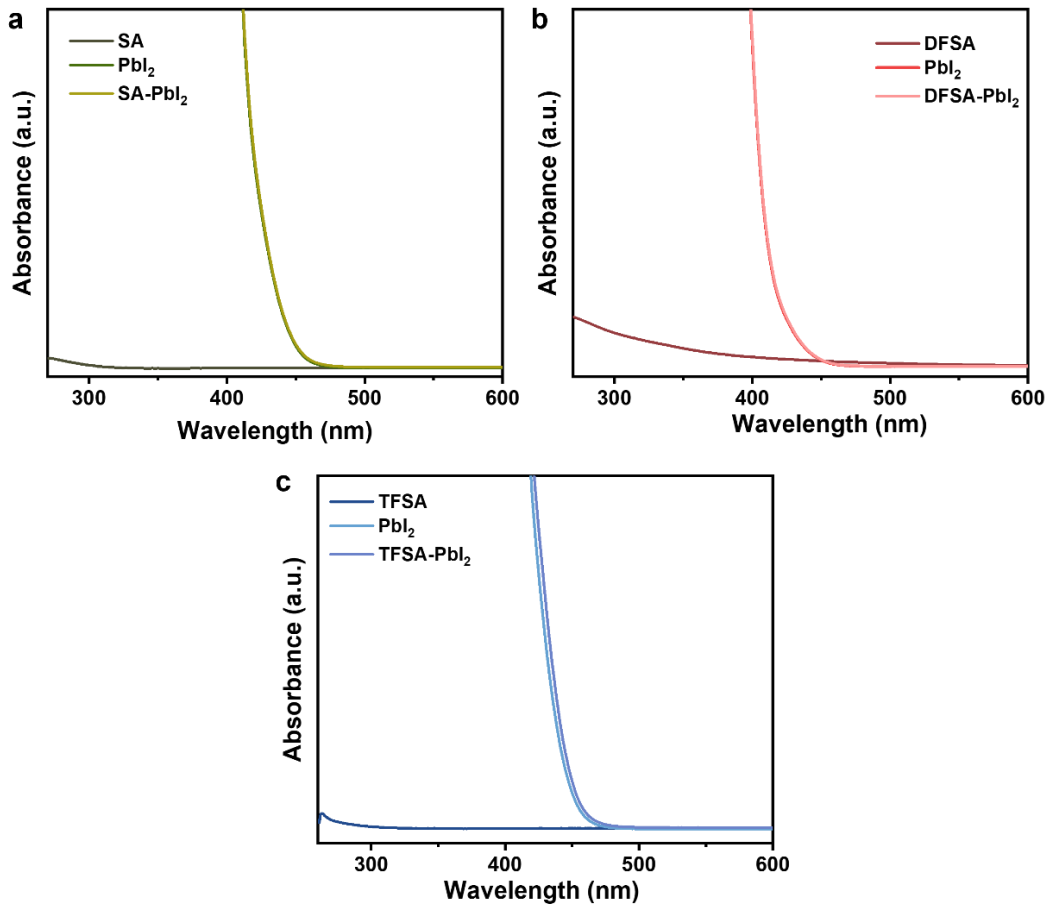

Fig. S4. The UV-vis absorption spectra of (a) SA, (b) DFSA, and (c) TFSA mixed with PbI_2, respectively. (Solvent: DMF: DMSO = 4:1).

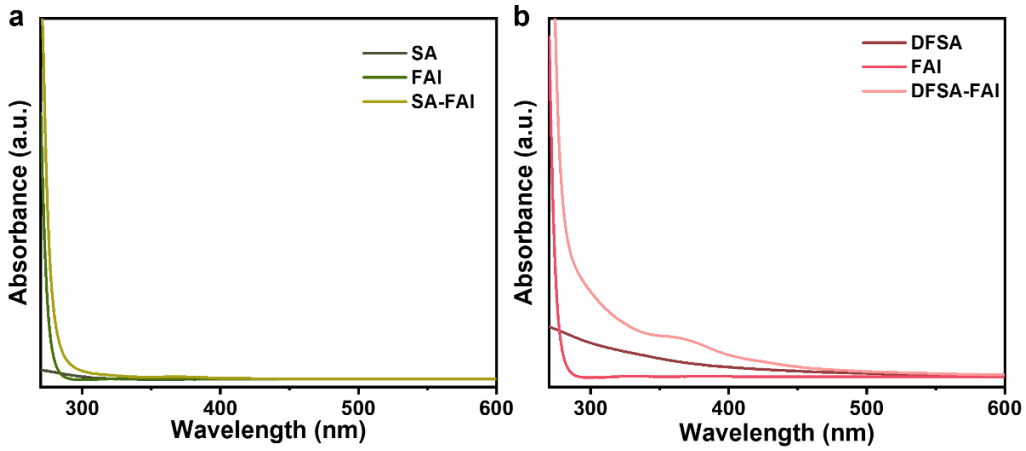

Fig. S5. The UV-vis absorption spectra of (a) DFSA, FAI, and DFSA-FAI samples, (b) SA, FAI, and SA-FAI samples (Solvent: DMF: DMSO = 4:1).

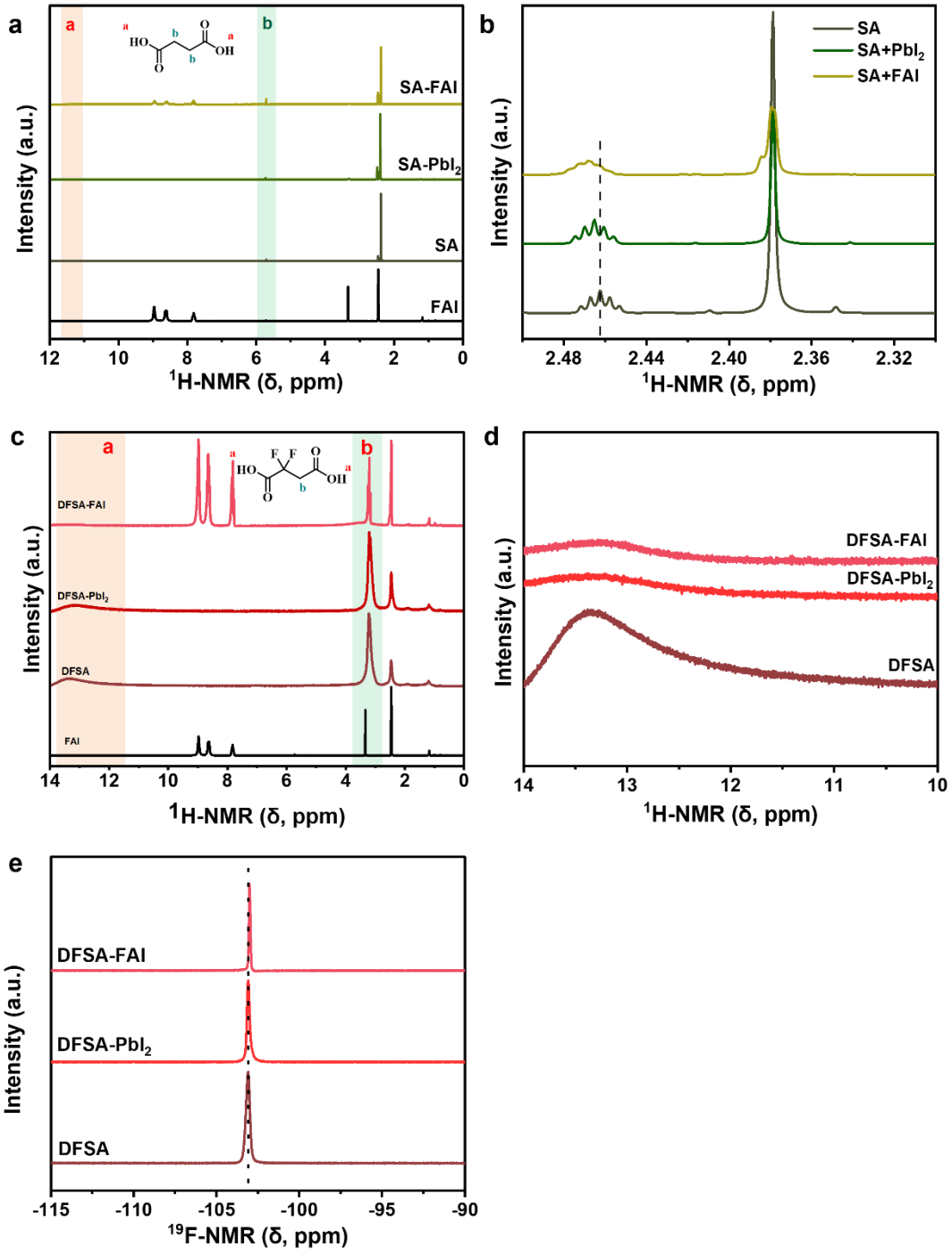

Fig. S6. (a) The ^{1}H-NMR spectra of SA, FAI, SA-FAI, and SA-PbI_2. (b) Partial enlarged ^{1}H-NMR spectra of SA, SA-FAI, and SA-PbI_2. (c) The ^{1}H-NMR spectra of DFSA, FAI, DFSA-FAI, and DFSA-PbI_2. (d) Partial enlarged ^{1}H-NMR spectra of DFSA, DFSA-FAI, and DFSA-PbI_2. (e) ^{19}F-NMR spectra of DFSA, DFSA-FAI, and DFSA-PbI_2 (solvent: DMSO-*d6*).

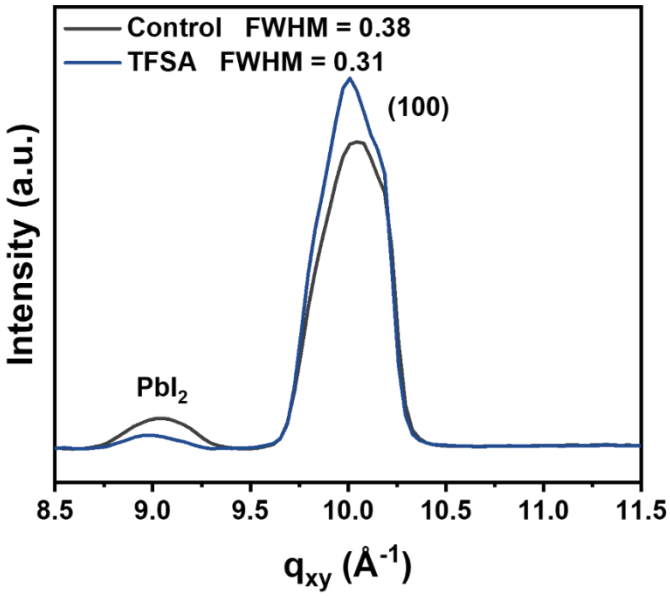

Fig. S7. 1D GIWAXS patterns of the control and TFSA-modified perovskite films (exposed the buried surface) extracted from the corresponding 2D GIWAXS patterns.

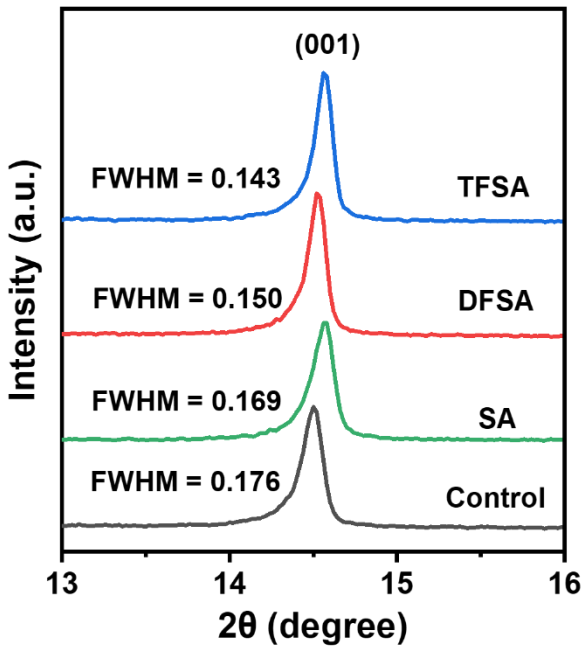

Fig. S8. The XRD patterns of (001) peak in perovskite films (exposed the buried surfaces) without and with SA derivatives treatment.

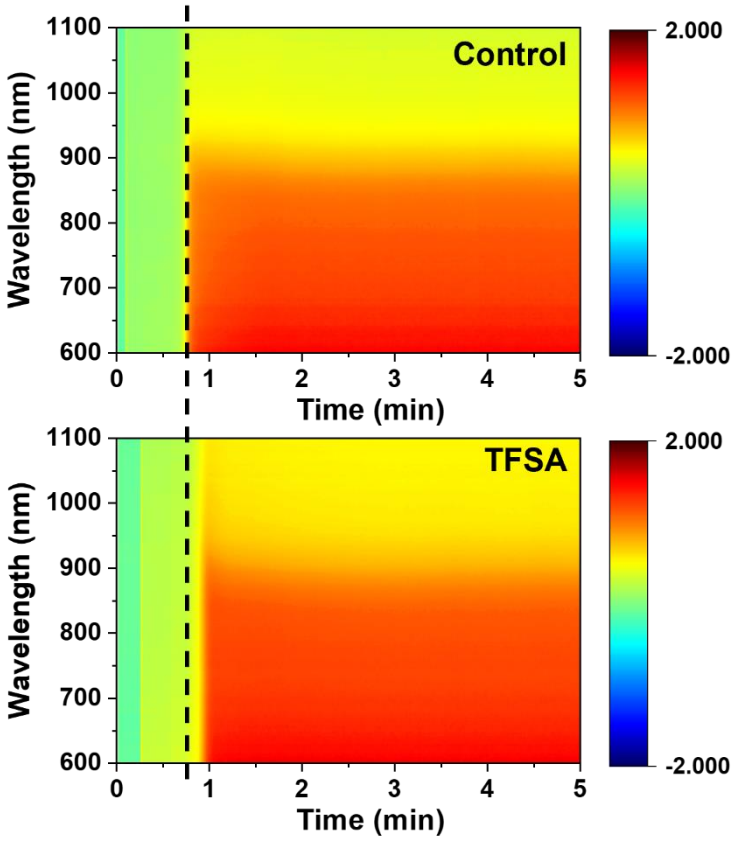

Fig. S9. Time evolution of in-situ UV-vis absorption spectra of the control and TFSA-mediated perovskites upon thermal annealing.

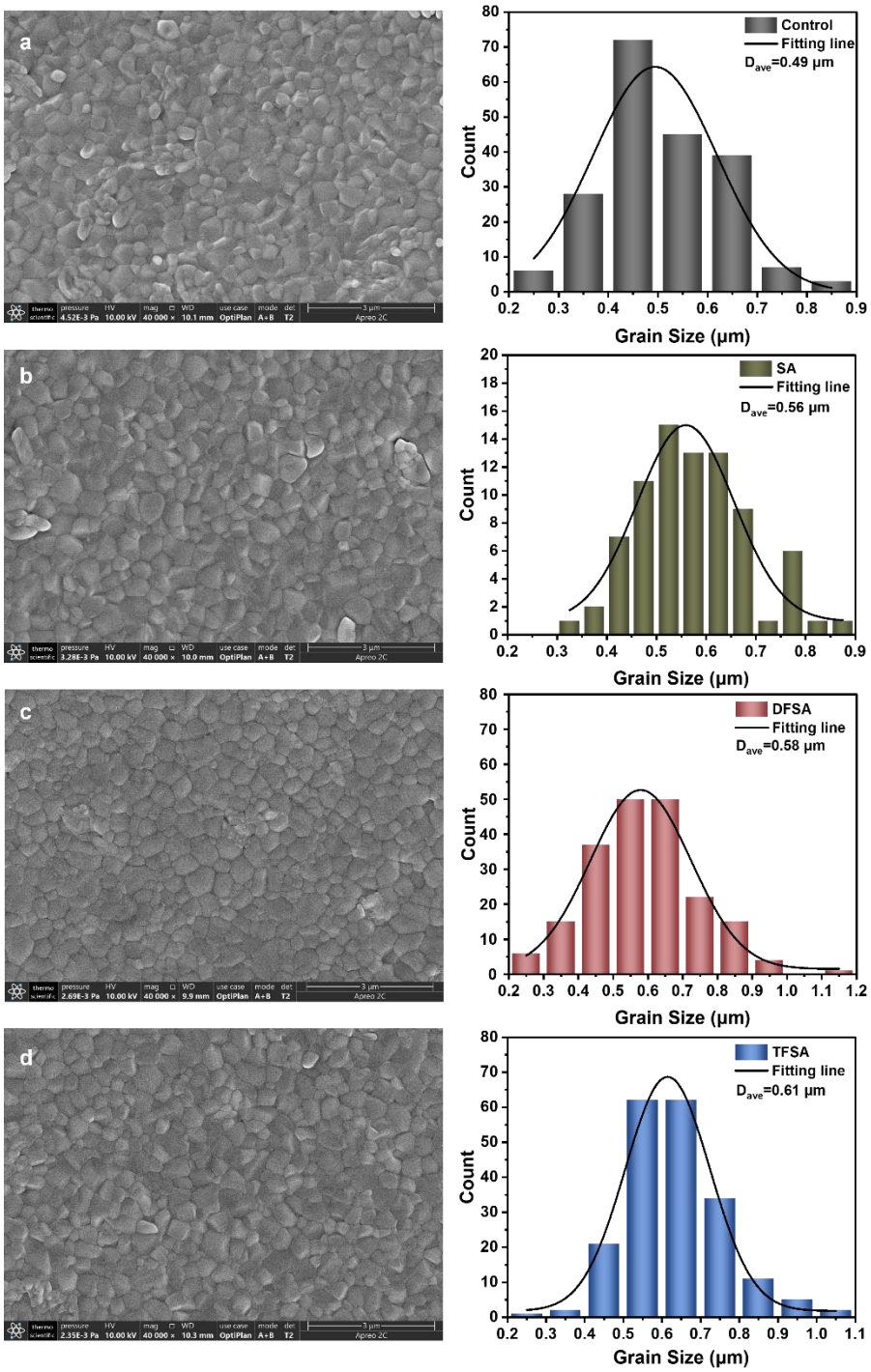

Fig. S10. Top-viewed of SEM images (left) and the statistical distribution of grain size (right) of perovskite films deposited on (a) control, (b) SA, (c) DFSA and (d) TFSA modified substrates, respectively.

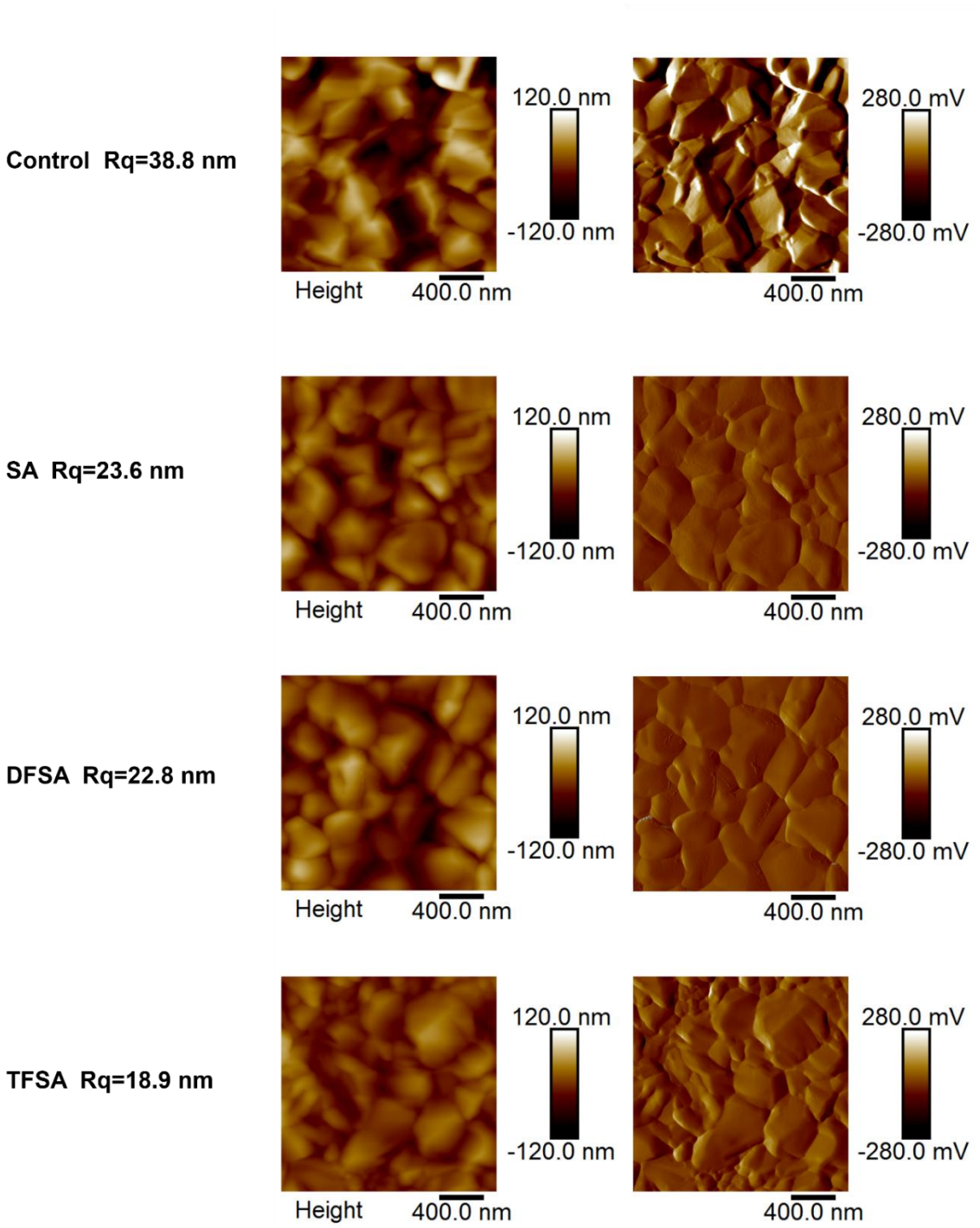

Fig. S11. AFM images of control, SA-, DFSA-, and TFSA-treated perovskite films, and the root mean square of their surface roughness, respectively.

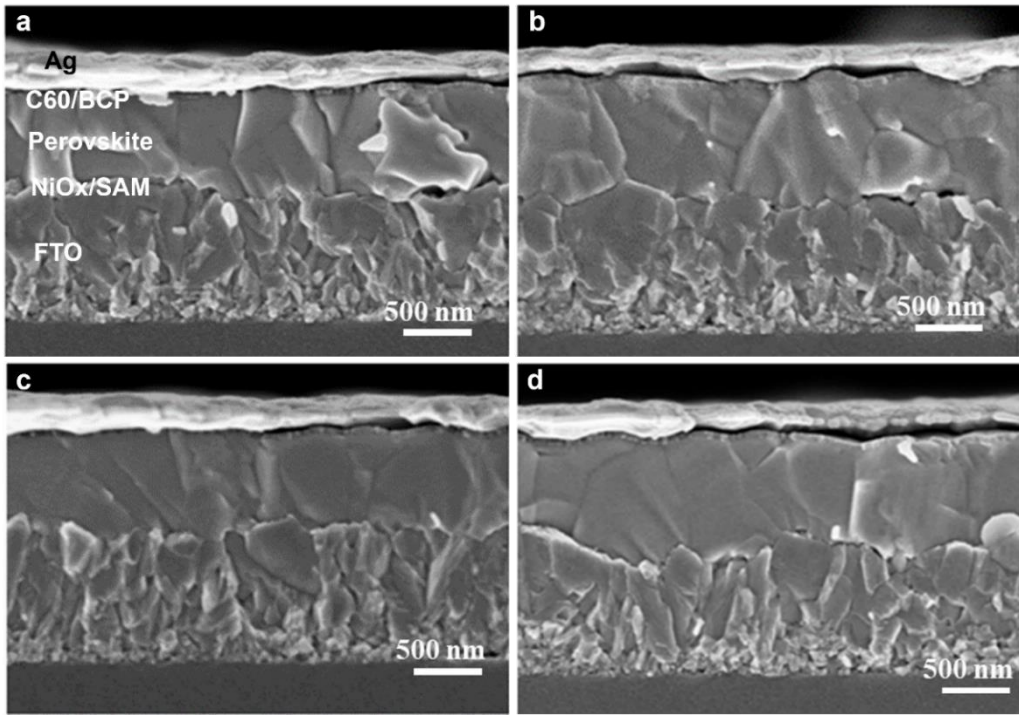

Fig. S12. Cross-sectional of SEM images of perovskite films deposited on (a) control, (b) SA, (c) DFSA and (d) TFSA modified substrates, respectively.

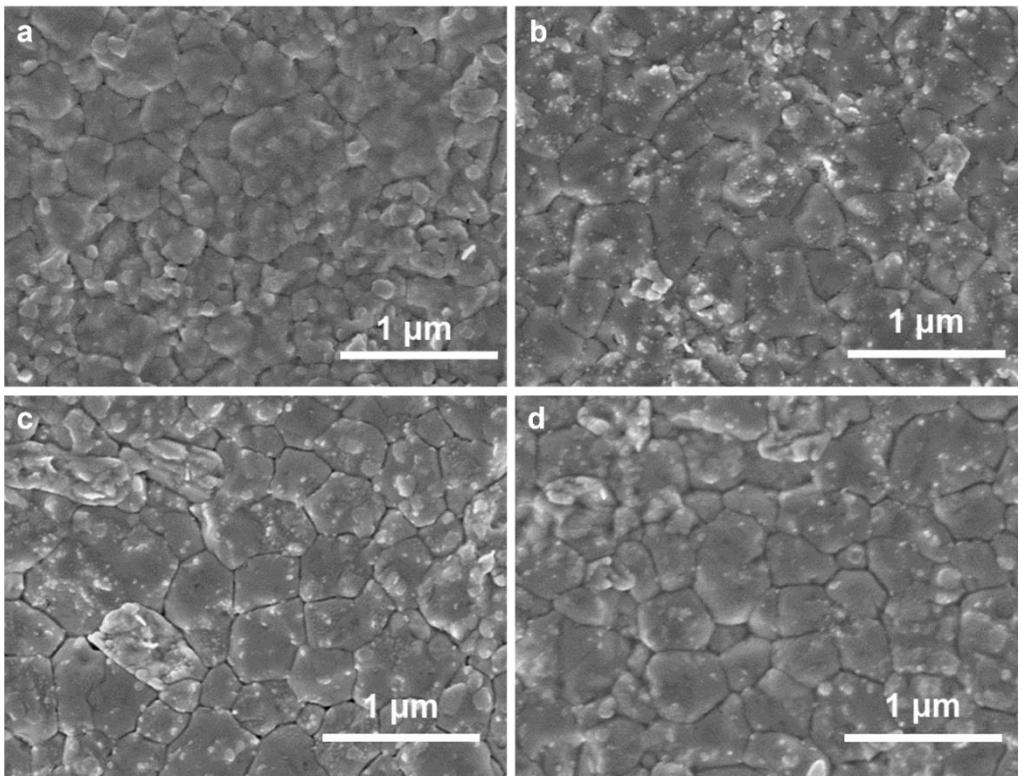

Fig. S13. SEM images of the buried perovskite films surface deposited on (a) control, (b) SA, (c) DFSA and (d) TFSA modified substrates.

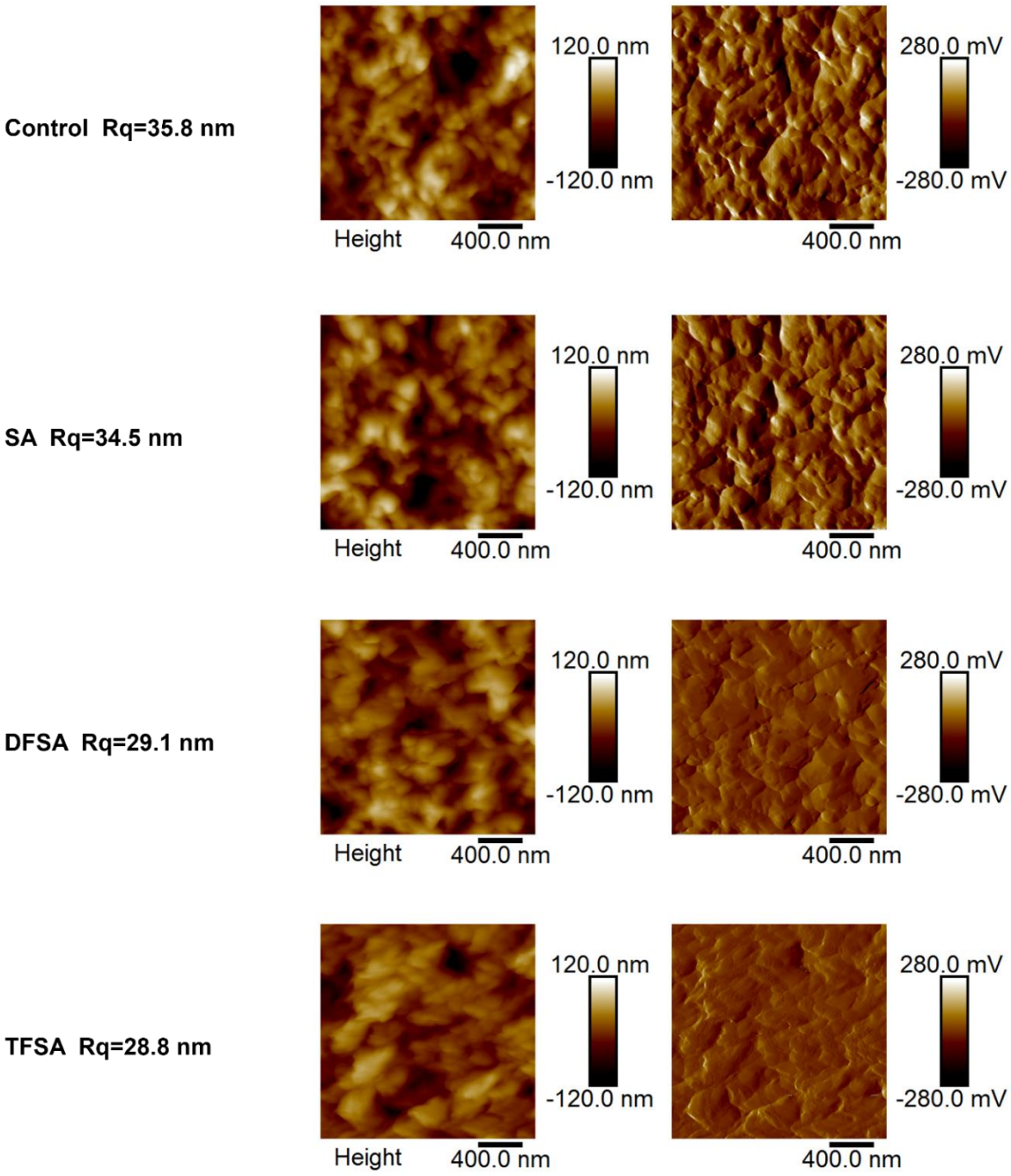

Fig. S14. AFM images of the buried surface for the control, SA-, DFSA- and TFSA-treated perovskite films, and the corresponding roughness.

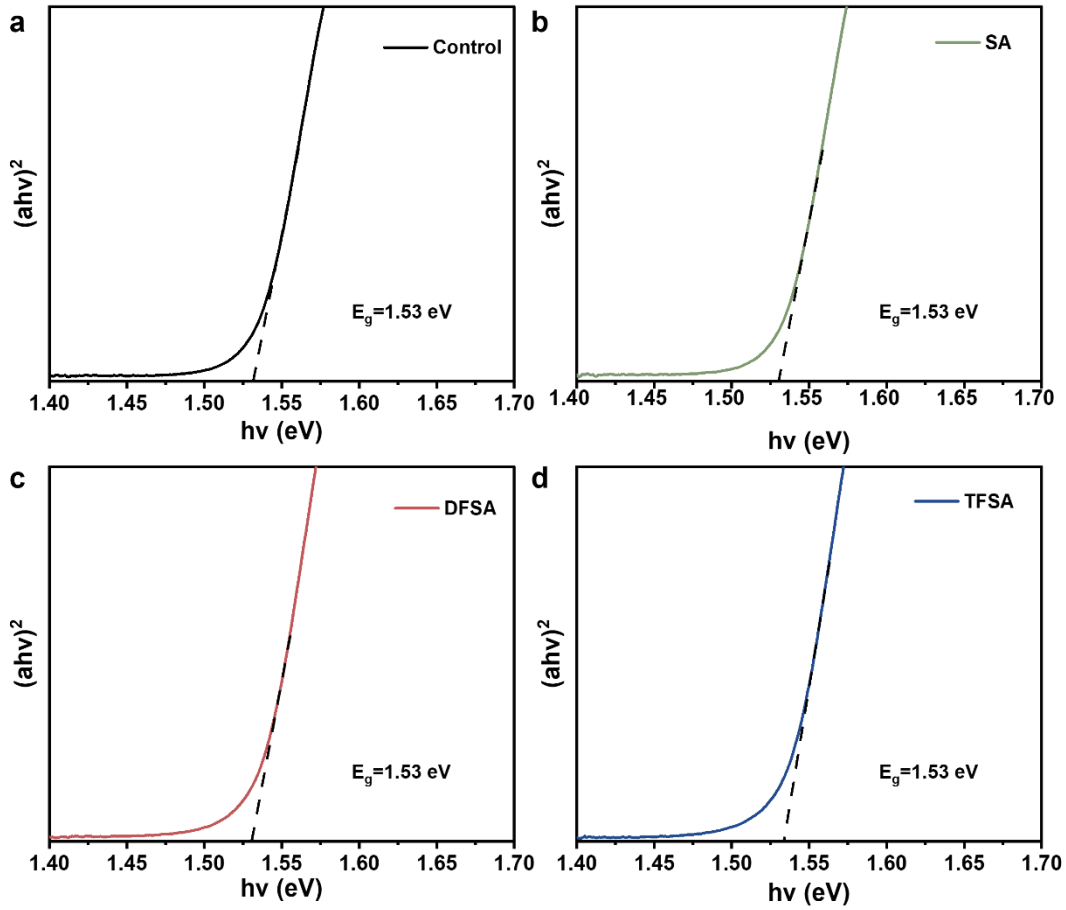

Fig. S15. Tauc plots of the perovskite films based on (a) control, (b) SA, (c) DFSA, and (d) TFSA treatment extracted from UV-vis absorption spectra.

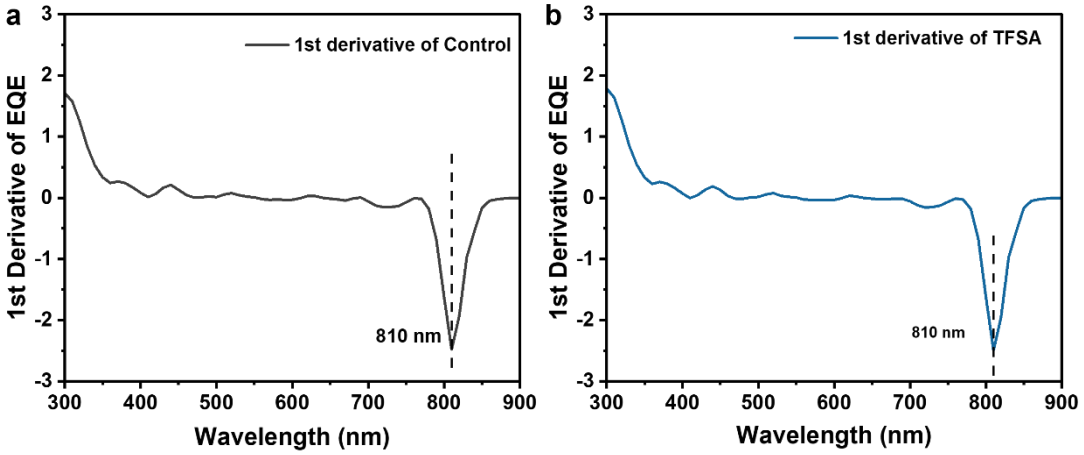

Fig. S16. The first derivative of EQE for (a) the control and (b) TFSA-based devices.

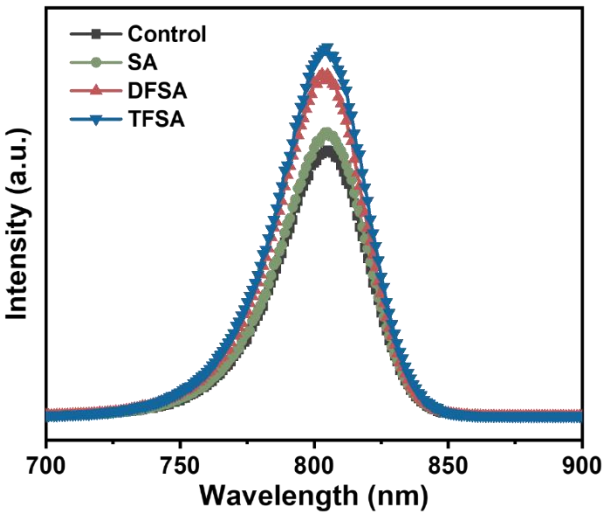

Fig. S17. The steady-state photoluminescence spectra of control, SA, DFSA, and TFSA-based perovskite films.

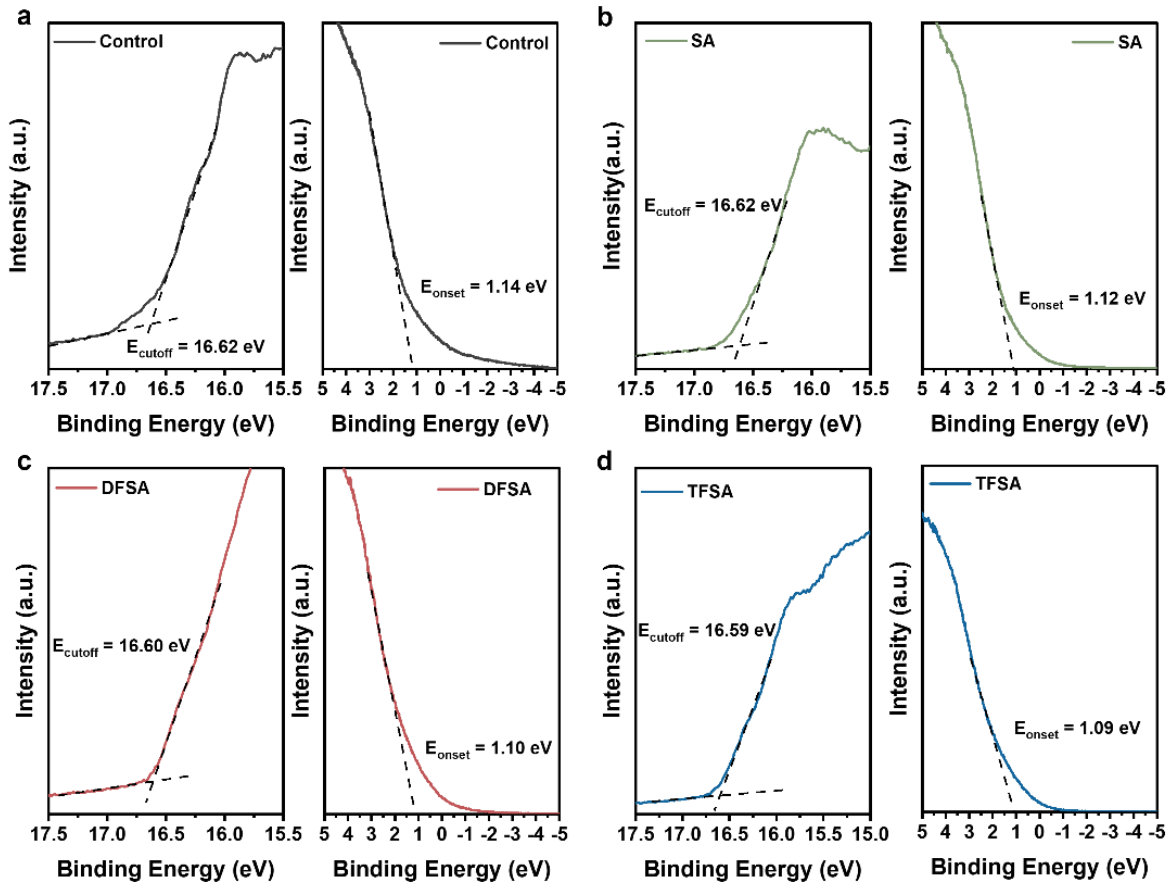

Fig. S18. UPS spectra of (a) control, (b) SA-, (c) DFSA-, and (d) TFSA-treated perovskite films.

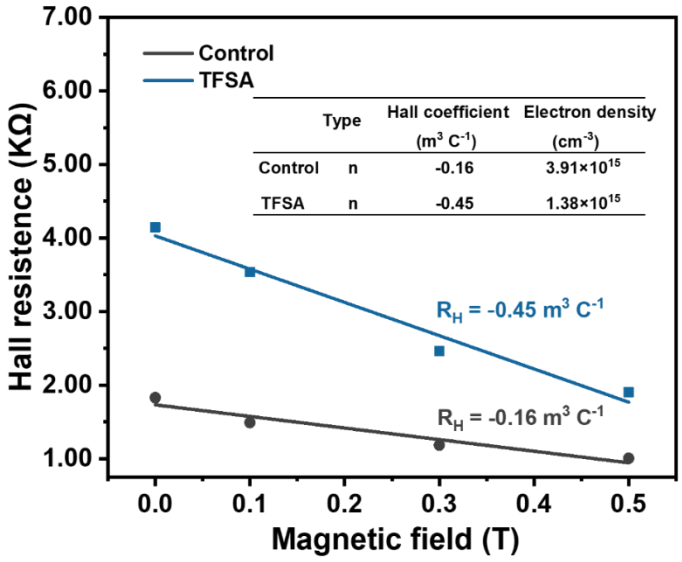

Fig. S19. Hall effect measurement of perovskite films without and with TFSA treatment.

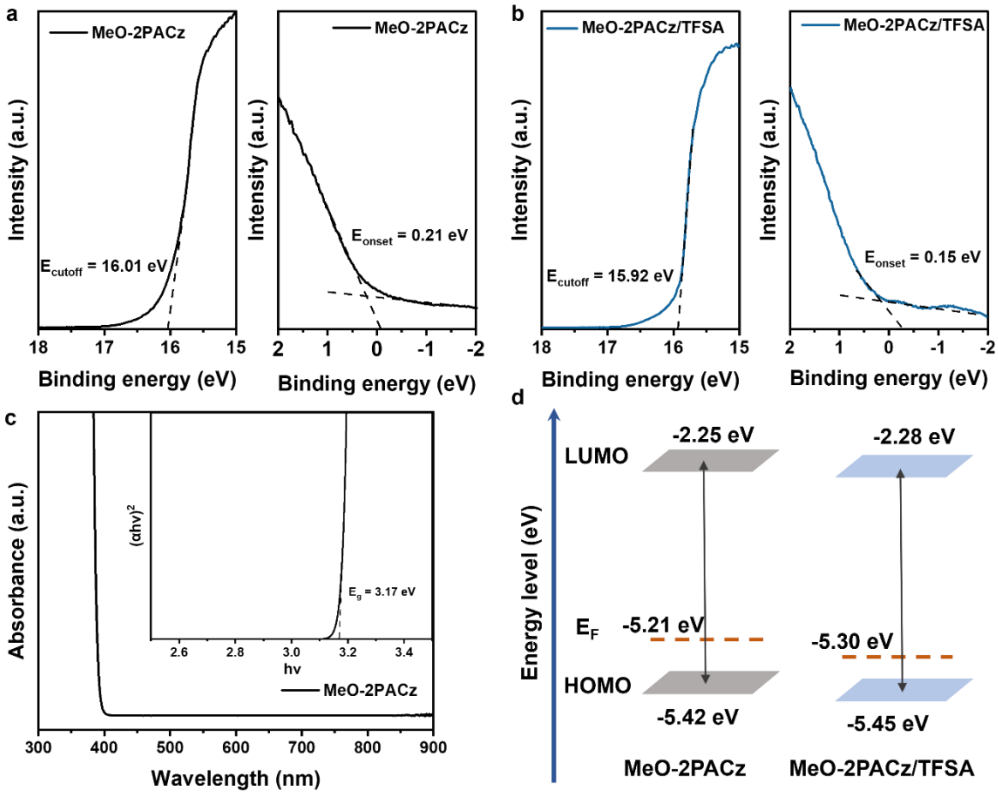

Fig. S20. UPS spectra of (a) MeO-2PACz and (b) MeO-2PACz/TFSA films. (c) UV-vis absorption spectrum and the bandgap of MeO-2PACz. (d) The energy levels for MeO-2PACz without and with TFSA treatment.

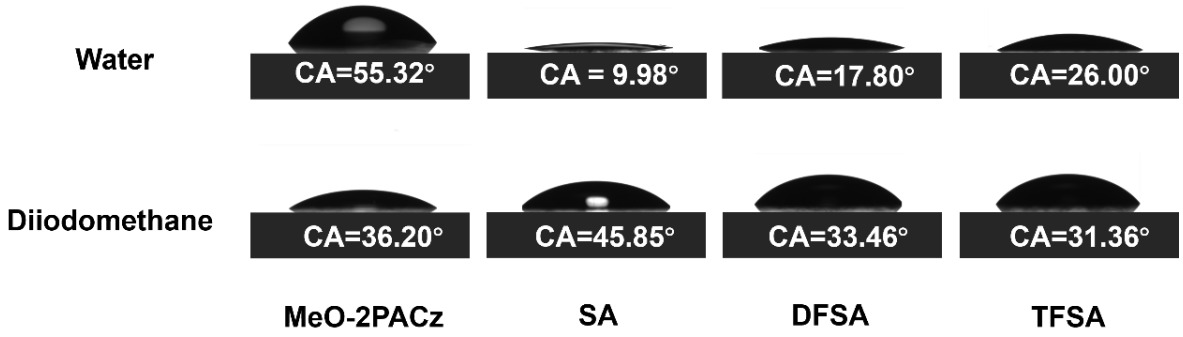

Fig. S21. The contact angle (CA) of water/diiodomethane based on MeO-2PACz substrates without and with SA derivatives treatment.

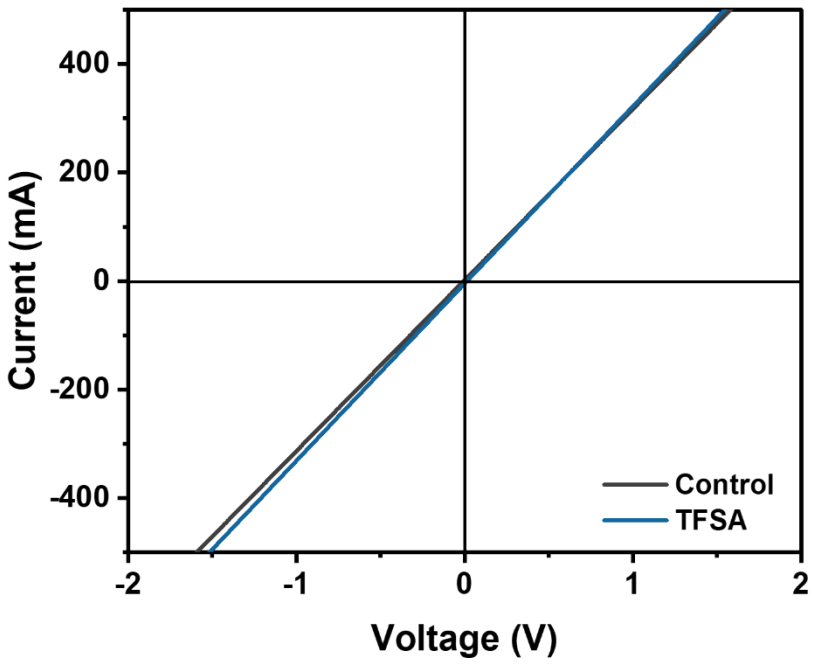

Fig. S22. Conductivities of NiOx/MeO-2PACz (control) and NiOx/MeO-2PACz/TFSA (TFSA) films.

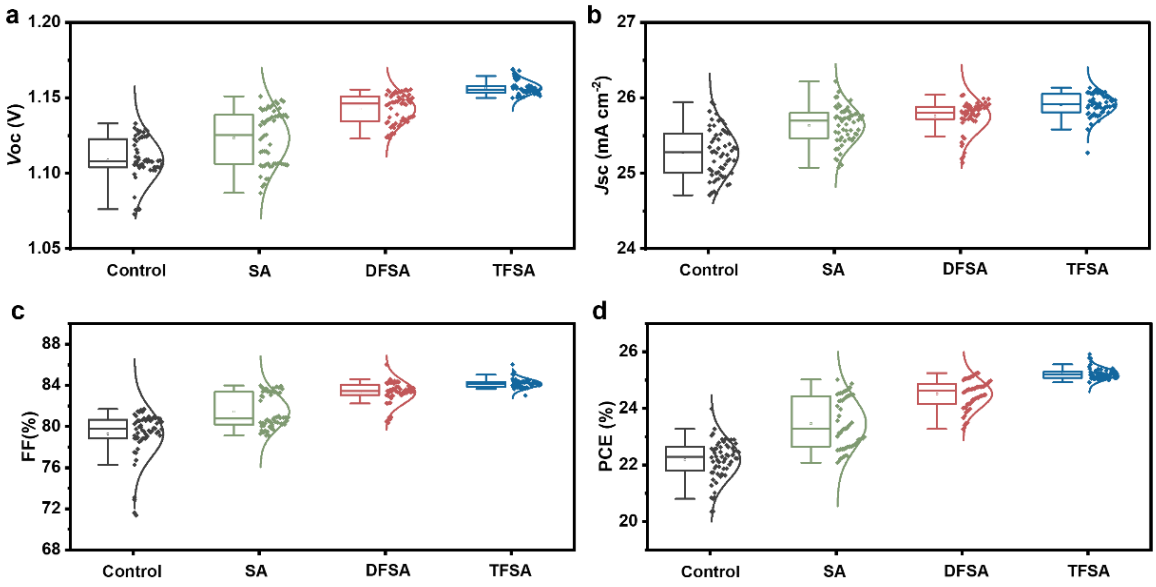

Fig. S23. Statistics of the PV parameters for 60 individual devices without and with SA derivatives treatment.

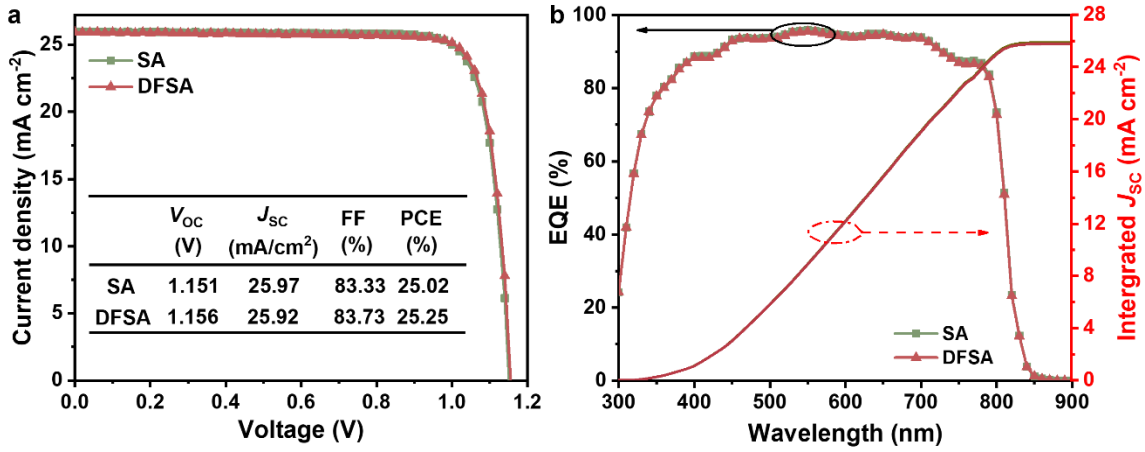

Fig. S24. (a) *J-V* curves of the SA and DFSA-based devices. (b) EQE curves and the corresponding integrated current densities of the SA- (25.88 mA/cm^2) and DFSA-treated (25.78 mA/cm^2) devices.

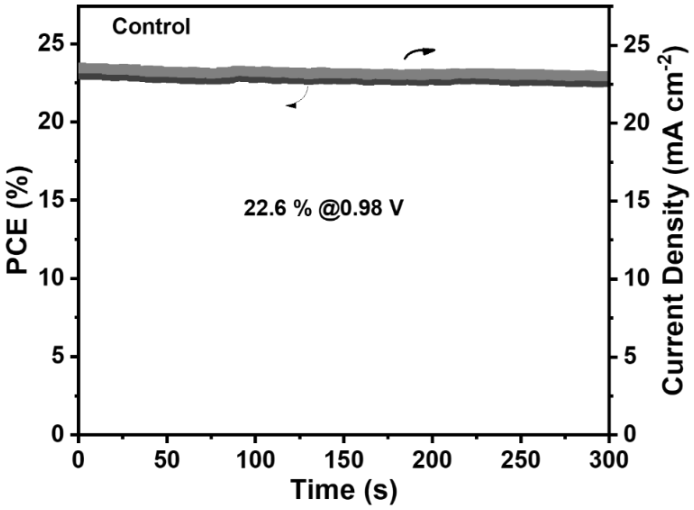

Fig. S25. The steady-state output power curve of the control device under standard 1-sunlight for 300 s.

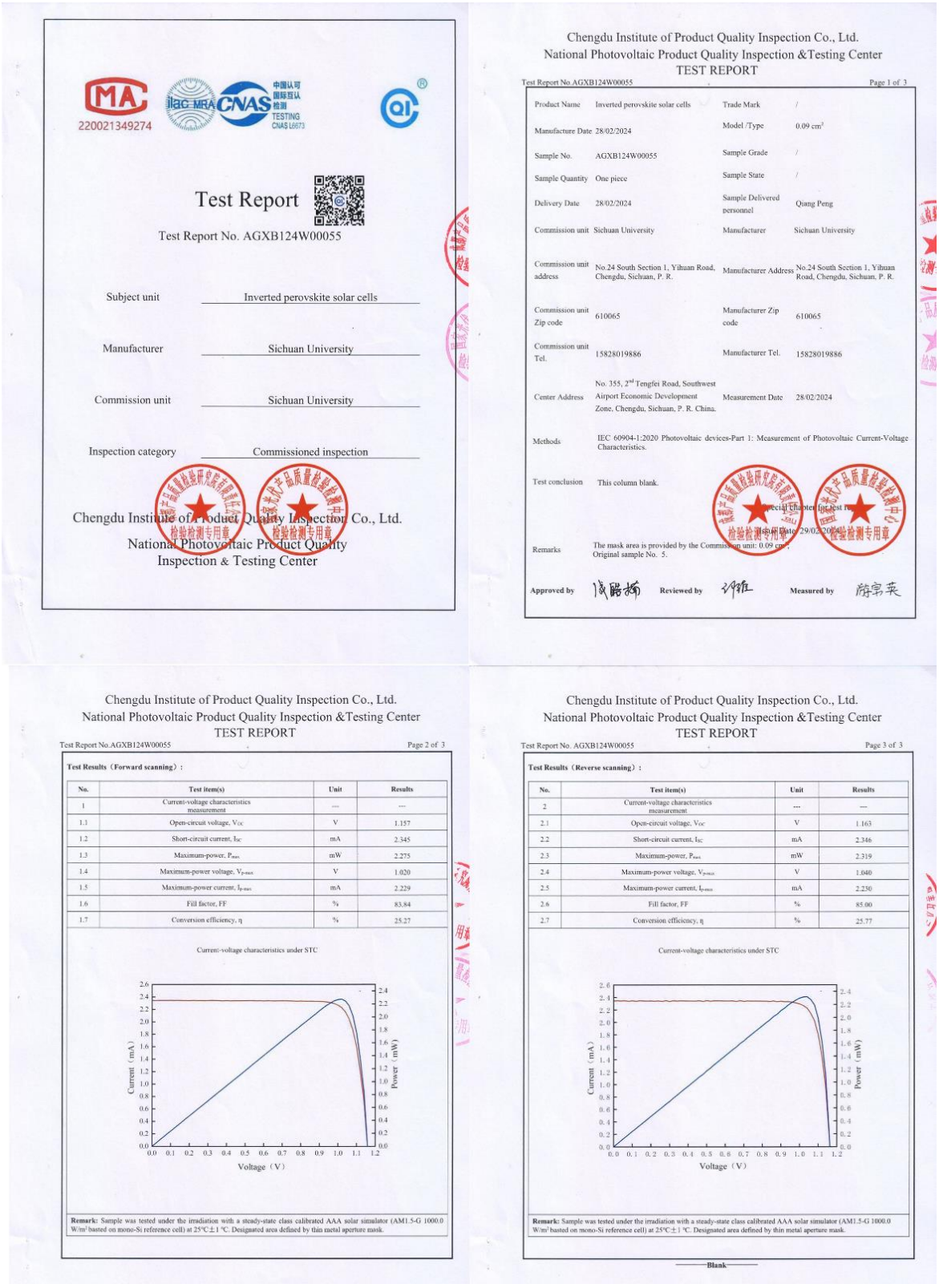

Fig. S26. The certification report of photovoltaic performance of the TFSA-treated perovskite solar cell (aperture area: 0.09 cm^2) with forward and reverse scan from National Photovoltaic Product Quality Inspection & Testing Center, China.

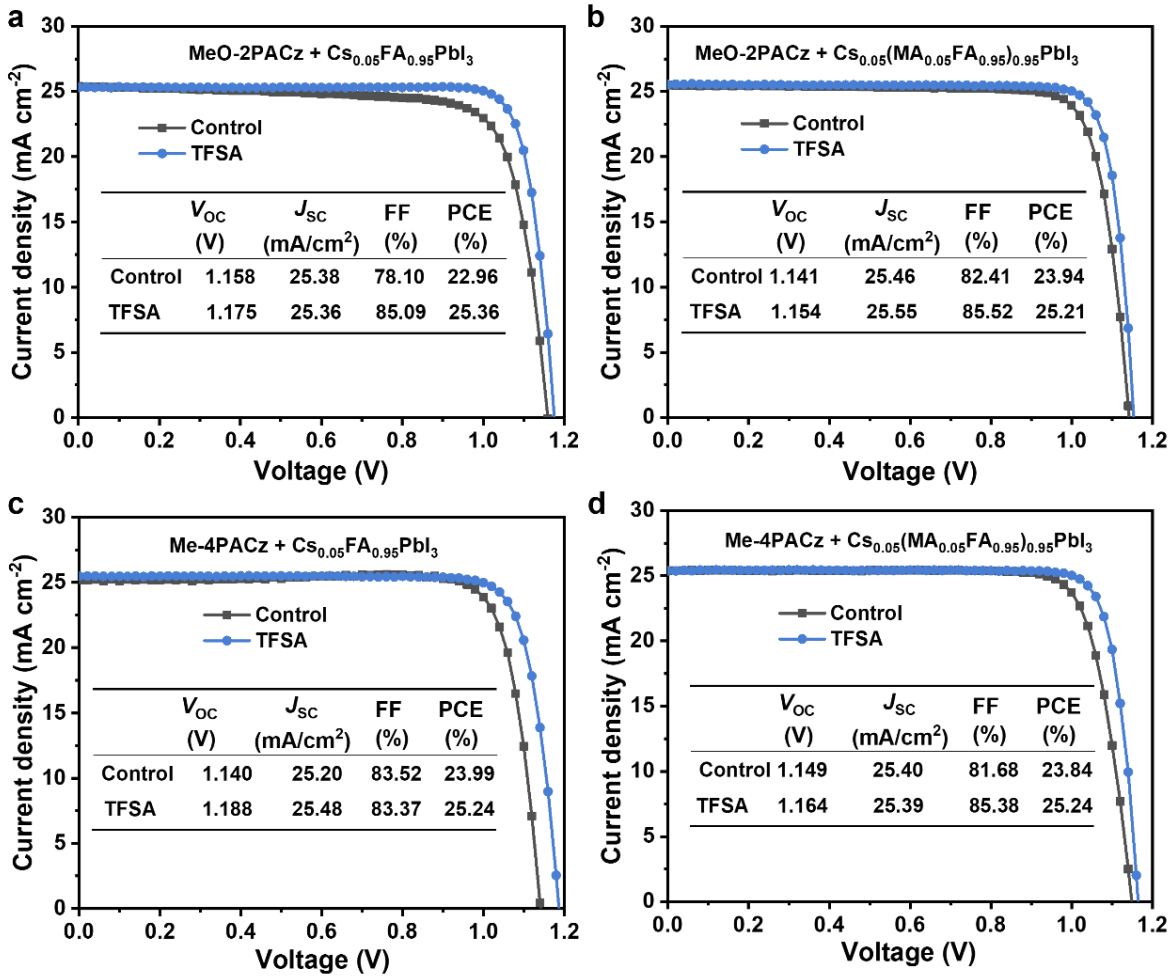

Fig. S27. *J-V* curves of the optimized control and TFSA based devices with different SAMs and perovskite compositions: MeO-2PACz combined with (a) CsFA- and (b) CsFAMA-based perovskites. Me-4PACz combined with (c) CsFA- and (d) CsFAMA-based perovskites.

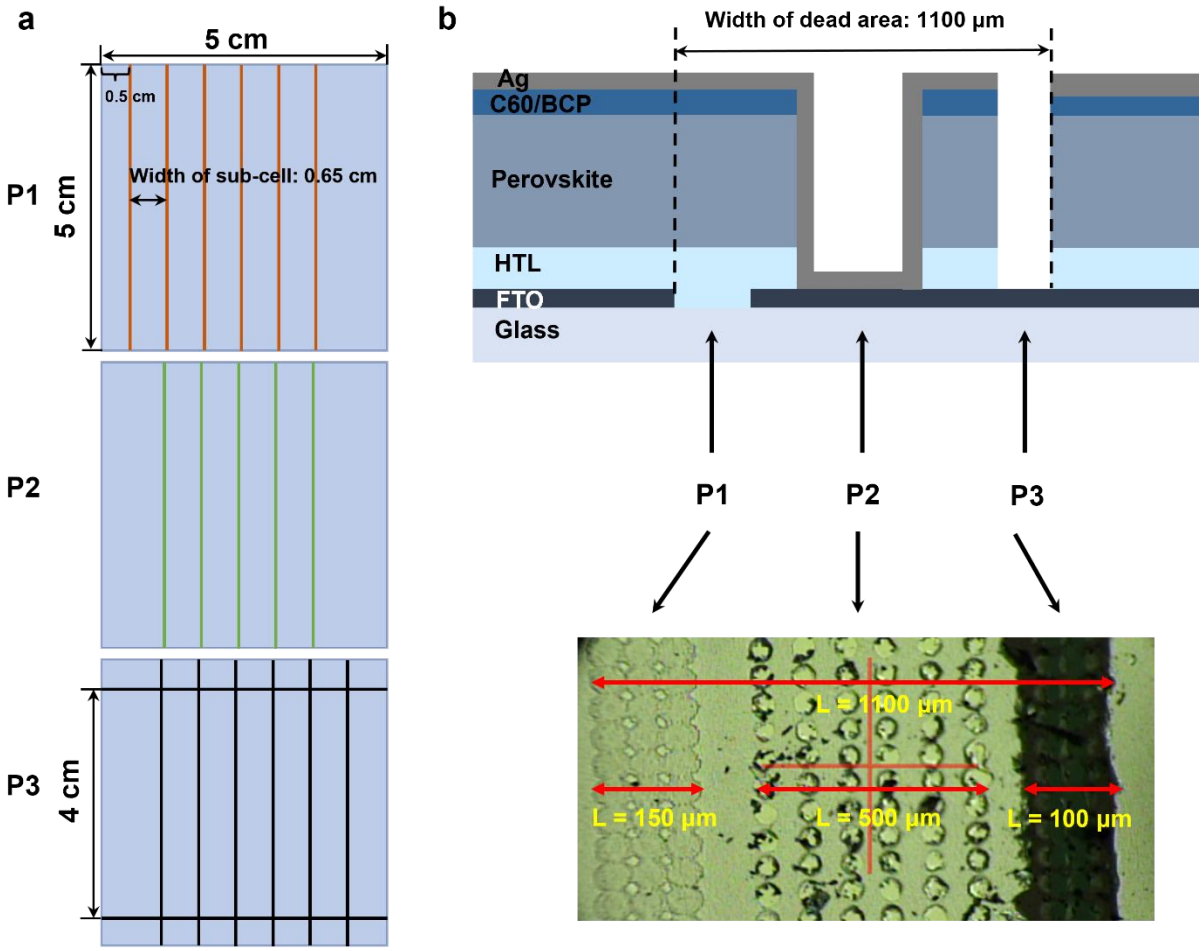

Fig. S28. (a) The illustration of the laser scribe process for the designed perovskite solar minimodule. (b) The micrograph of the dead area (P1, P2, and P3 scribes) for the minimodule. The width of each sub-cell is 6500 μm, while the width for a single dead area is 1100 μm. Therefore, the GFF was calculated to be 83.08%. After subtracting the dead area, the whole active area was calculated to be 12.96 cm^2 for the minimodule.

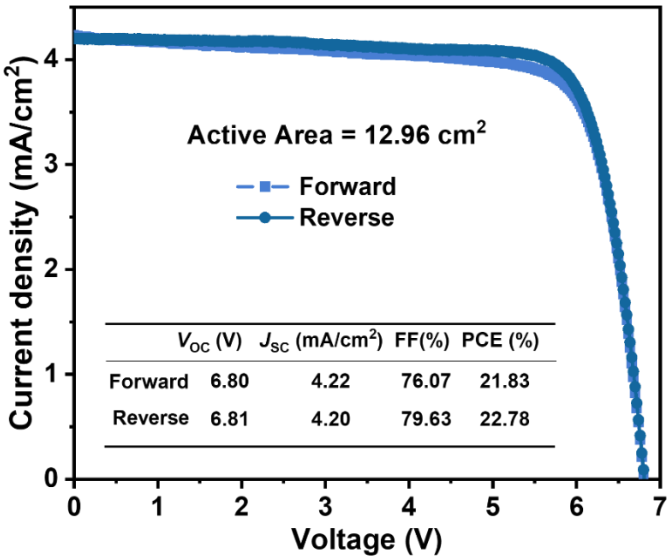

Fig. S29. The *J-V* curve of the forward and reverse scan of the target mini-module with 12.96 cm^2 of active area.

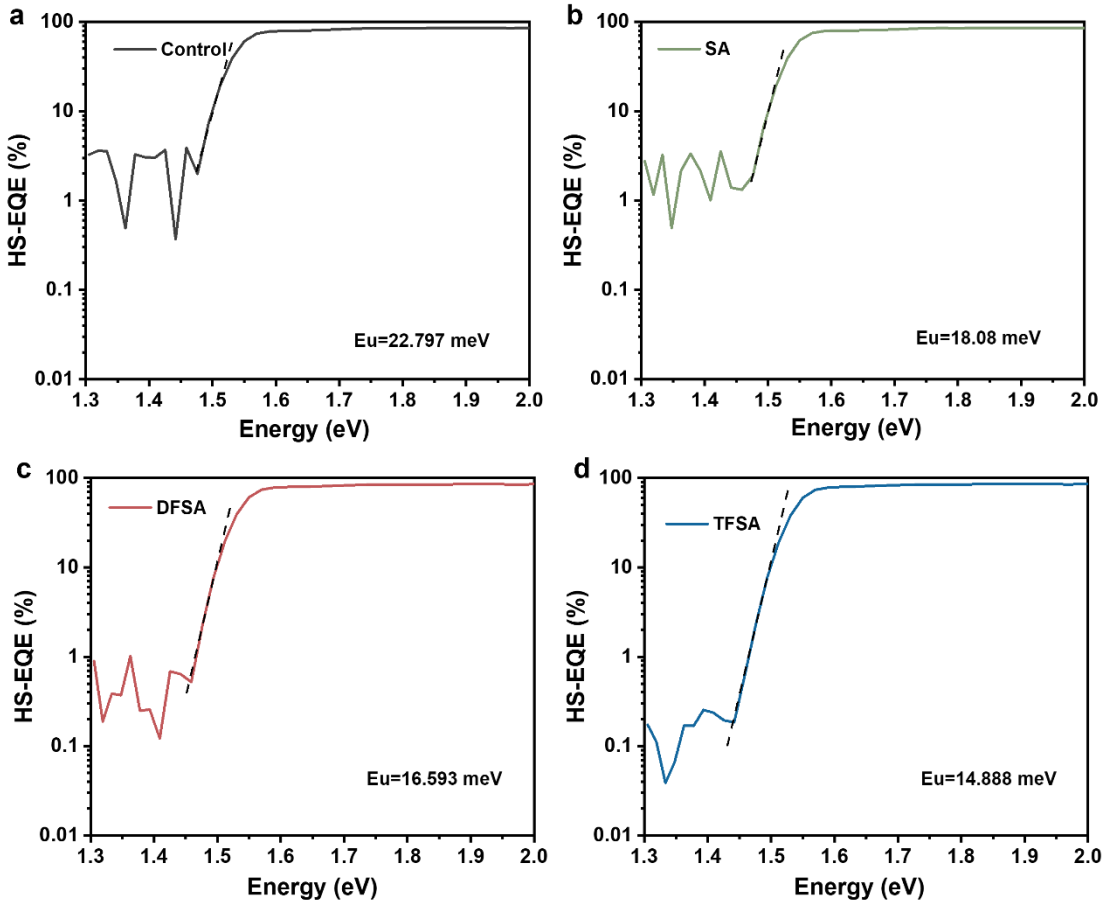

Fig. S30. Urbach energy (Eu) curves of (a) control, (b) SA-, (c) DFSA-, and (d) TFSA-treated devices, respectively.

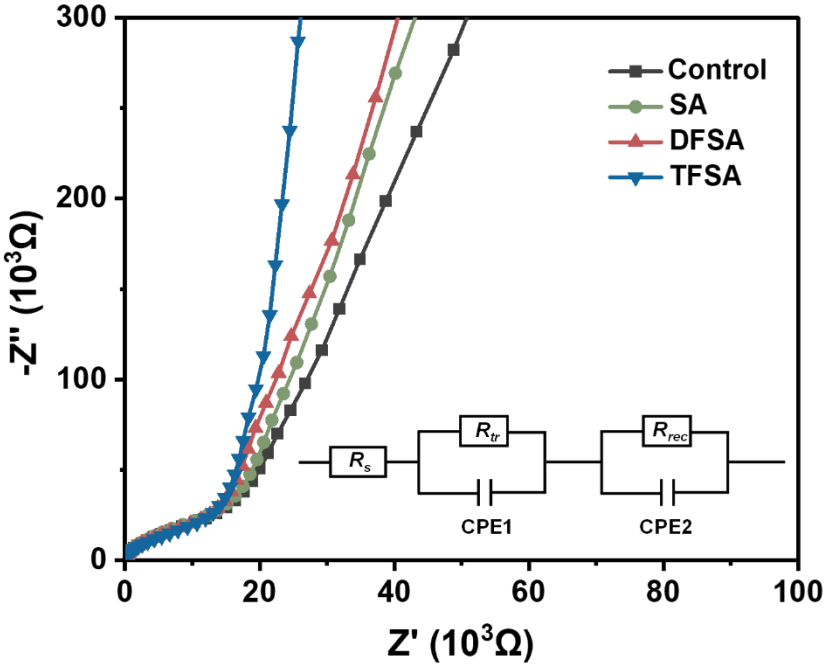

Fig. S31. EIS for the devices without and with SA derivatives treatment.

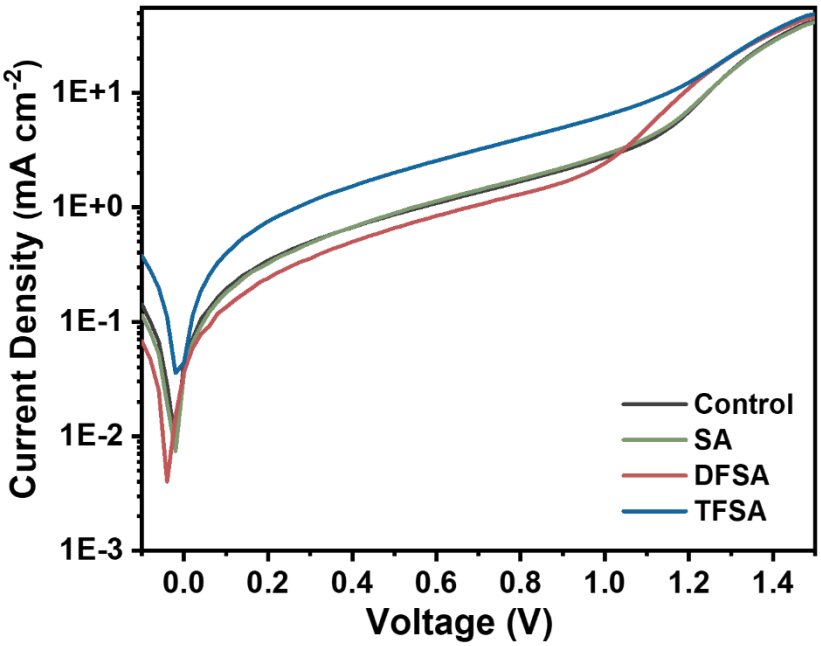

Fig. S32. Dark *J-V* curves of without and with SA derivatives treatment.

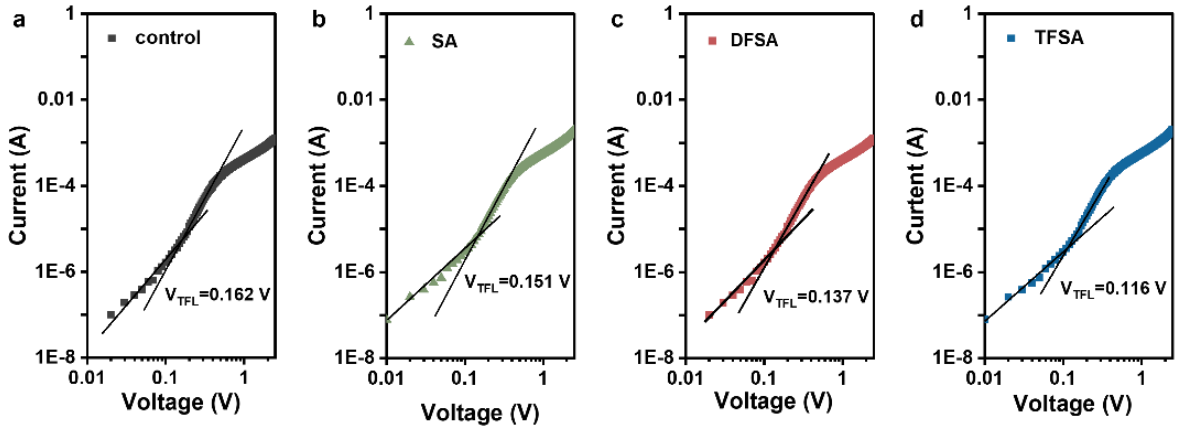

Fig. S33. Dark I-V curves of the hole-only devices based on the (a) control, (b) SA-, (c) DFSA-, and (d) TFSA-treated devices.

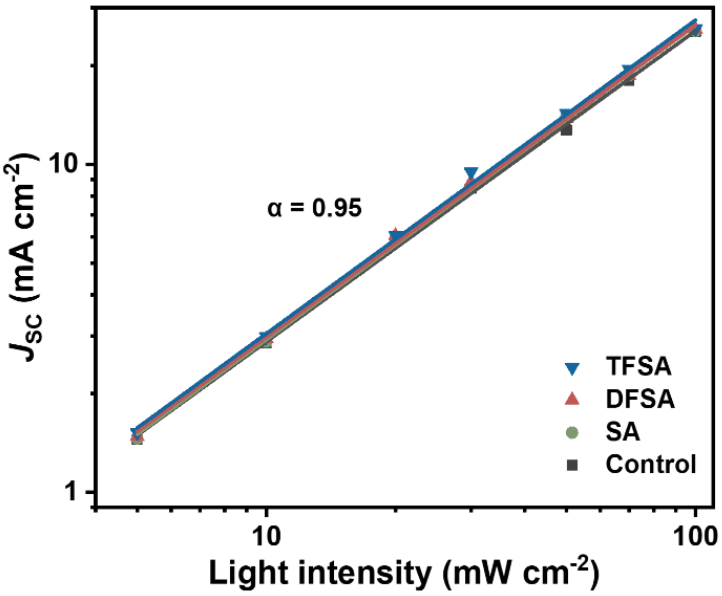

Fig. S34. J_{SC} vs. light intensity for the devices without and with SA derivatives treatment.

Table S1. Summary of PV parameters for inverted PSCs based on RbCsFAMA quadruple cation perovskites.

Devices Configurations	Eg (eV)	Scan direction	V_{OC} (V)	J_{SC} (mA/cm^2)	FF (%)	PCE (%)	Ref.
ITO/PTAA/$Rb_{0.025}Cs_{0.025}FA_{0.7}MA_{0.25}PbI_3$/$CdI_2$/C60/BCP/Cu	1.51	Reverse	1.200	23.50	77.70	21.90	2
		Forward	1.200	23.30	77.60	21.70	
ITO/PTAA/$Rb_{0.05}Cs_{0.05}FA_{0.85}MA_{0.05}PbI_{2.85}Br_{0.15}$/C60/BCP/Cu	N/A	Reverse	1.150	23.40	81.70	22.00	3
		Forward	/	/	/	/	
FTO/NiOx/$Rb_{0.2}Cs_{0.2}FA_{0.3}MA_{0.3}$/$PC_{61}BM$/BCP/Ag	1.63	Reverse	1.250	23.70	77.00	22.81	4
		Forward	/	/	/	/	
ITO/PTAA/$Rb_{0.05}Cs_{0.05}FA_{0.79}MA_{0.16}PbI_{1.8}Br_{1.2}$/SG/$PC_{61}BM$/BCP/Ag	1.78	Reverse	1.190	18.53	80.30	17.71	5
		Forward	1.190	18.62	79.30	17.57	
ITO/PTAA: BDT-Si/$Rb_{0.05}Cs_{0.05}FA_{0.8}MA_{0.1}PbI_{2.85}Br_{0.15}$/$PC_{61}BM$/BCP/Cu	1.53	Reverse	1.100	24.44	81.37	21.87	6
		Forward	/	/	/	/	
ITO/MeO-2PACz/$Rb_{0.05}Cs_{0.05}FA_{0.85}MA_{0.05}PbI_{2.85}Br_{0.15}$/LiF/C60/BCP/Ag	1.53	Reverse	1.150	26.13	84.60	25.49	7
		Forward	1.150	26.19	83.90	25.27	
ITO/MeO-2PACz/$Rb_{0.05}Cs_{0.05}FA_{0.85}MA_{0.05}PbI_{2.85}Br_{0.15}$/C60/BCP/Ag	1.54	Reverse	1.195	24.85	84.27	25.03	8
		Forward	1.191	24.87	82.42	24.42	
FTO/MeO-2PACz/$Rb_{0.05}Cs_{0.05}FA_{0.85}MA_{0.05}PbI_{2.85}Br_{0.15}$/$PC_{61}BM$/BCP/Ag	1.55	Reverse	1.184	25.40	83.41	25.09	9
		Forward	1.184	25.38	83.00	24.96	
FTO/MeO-2PACz/$Rb_{0.05}Cs_{0.05}FA_{0.85}MA_{0.05}PbI_{2.85}Br_{0.15}$/LiF/C60/BCP/Ag	1.54	Reverse	1.159	26.13	82.00	24.80	10
		Forward	1.157	26.22	81.00	24.54	
ITO/MeO-2PACz/$Rb_{0.05}Cs_{0.05}MA_{0.05}FA_{0.85}Pb(I_{0.95}Br_{0.05})_3$/C60/$SnO_2$/Ag	1.53	Reverse	1.18	25.58	84.9	25.58	11
		Forward	1.18	25.62	84.5	25.49	
ITO/PTAA/$(Rb_{0.05}Cs_{0.05}MA_{0.05}FA_{0.85})Pb(I_{0.95}Br_{0.05})$/$PC_{61}BM$/BCP/Cu	1.55	Reverse	1.147	25.03	82.7	23.74	12
		Forward	1.146	25.37	79.54	23.13	
ITO/MeO-2PACz/$Rb_{0.05}Cs_{0.05}FA_{0.85}MA_{0.05}PbI_{2.85}Br_{0.15}$/C60/BCP/Ag	1.56	Reverse	1.18	24.45	83.4	24.06	13
		Forward	1.18	24.31	80.0	22.95	
FTO/NiO_x/MeO-2PACz/$RbCs_{0.05}MA_{0.05}FA_{0.90}PbI_3$/$PDAI_2$/C60/BCP/Ag	**1.53**	**Reverse**	**1.169**	**26.07**	**85.06**	**25.92**	**This work**
		Forward	**1.161**	**26.08**	**83.49**	**25.28**	

Table S2. TRPL lifetimes of perovskite films without and with SA derivatives treatment fitted from the decay curves by a biexponential model.

Samples	τ_1 (ns)	A_1	τ_2 (ns)	A_2	τ_{ave} (ns)
Control	129.12	0.33	1002.01	0.68	950.6361
SA	82.1	0.35	2241.76	0.76	2205.94
DFSA	105.71	0.47	2411.21	0.66	2341.411
TFSA	122.37	0.33	3482.01	0.73	3429.471

Table S3. Flory-Huggins interaction parameters (χ) of MeO-2PACz/buried interface passivators and the corresponding parameters.

Material	Contact Angle (°)		γ^d	γ^p	Surface free energy	$\gamma_{MeO\text{-}2PACz/SA\ derivatives}$	Flory-Huggins interaction parameters (χ)
	Water	diiodomethane	[mN/m]	[mN/m]	[mN/m]	[mN/m]	
MeO-2PACz	55.32	36.2	41.47	14.34	55.81	/	/
SA	9.98	45.85	36.55	38	74.55	/	/
DFSA	17.8	51.45	33.46	38.04	71.51	/	/
TFSA	26	55.16	31.36	36.21	67.56	/	/
MeO-2PACz/SA	/	/	/	/	/	98.22	1.34
MeO-2PACz/DFSA	/	/	/	/	/	95.52	0.98
MeO-2PACz/TFSA	/	/	/	/	/	92.09	0.56

Table S4. PV parameters of 60 control devices.

Entry	V_{OC}(V)	J_{SC} (mAcm^{-2})	FF (%)	PCE (%)
1	1.064	25.82	79.11	21.73
2	1.073	25.16	78.84	21.28
3	1.076	25.33	79.77	21.74
4	1.076	25.36	80.23	21.89
5	1.076	25.39	80.40	21.96
6	1.076	25.70	80.54	22.27
7	1.076	25.51	80.56	22.11
8	1.084	25.65	81.19	22.58
9	1.095	25.94	79.35	22.53
10	1.097	25.71	79.97	22.56
11	1.099	25.63	80.11	22.57
12	1.102	25.46	79.93	22.43
13	1.102	25.42	79.61	22.30
14	1.102	25.30	79.51	22.17
15	1.104	24.92	78.83	21.68
16	1.104	25.52	80.64	22.71
17	1.104	25.55	80.80	22.79
18	1.104	25.45	80.56	22.63
19	1.104	25.08	79.24	21.94
20	1.104	25.69	80.74	22.91
21	1.104	25.53	80.94	22.82
22	1.105	24.76	78.92	21.60
23	1.105	24.98	78.51	21.68
24	1.106	24.71	76.27	20.84
25	1.106	25.01	79.05	21.87
26	1.106	25.05	77.50	21.48

27	1.106	25.72	80.56	22.92
28	1.107	24.74	76.73	21.02
29	1.108	24.73	80.71	22.11
30	1.108	25.34	80.89	22.71
31	1.108	25.30	80.80	22.64
32	1.108	25.24	80.32	22.46
33	1.108	25.53	80.81	22.86
34	1.108	25.27	79.60	22.29
35	1.108	25.12	79.43	22.11
36	1.109	25.18	79.58	22.22
37	1.109	25.58	80.74	22.89
38	1.109	25.26	79.84	22.36
39	1.109	24.88	77.44	21.37
40	1.109	25.22	79.80	22.32
41	1.110	25.79	80.46	23.04
42	1.111	25.03	77.80	21.64
43	1.114	25.63	72.88	20.81
44	1.116	25.57	73.12	20.86
45	1.119	24.88	78.60	21.88
46	1.121	24.91	78.82	22.02
47	1.122	24.84	81.03	22.59
48	1.123	24.97	78.85	22.11
49	1.124	25.01	81.47	22.90
50	1.124	25.06	79.35	22.35
51	1.124	25.16	79.47	22.48
52	1.124	25.28	71.61	20.36
53	1.125	24.85	81.41	22.76
54	1.126	25.35	71.37	20.36

55	1.127	24.95	79.12	22.24
56	1.127	25.12	81.61	23.11
57	1.128	25.00	78.84	22.23
58	1.128	25.33	81.45	23.27
59	1.129	24.95	79.75	22.45
60	1.129	25.17	80.82	22.98
Average	1.110±0.016	25.26±0.31	79.28±2.22	22.17±0.67

Table S5. PV parameters of 60 SA-treated devices.

Entry	V_{OC}(V)	J_{SC} (mAcm^{-2})	FF (%)	PCE (%)
1	1.151	25.96	83.73	25.01
2	1.148	25.72	83.35	24.60
3	1.148	25.82	83.95	24.87
4	1.145	25.71	83.36	24.53
5	1.148	25.87	83.28	24.75
6	1.146	25.85	83.20	24.65
7	1.145	25.81	82.90	24.49
8	1.144	25.79	83.08	24.50
9	1.142	25.77	82.96	24.42
10	1.143	25.77	83.78	24.68
11	1.142	25.52	83.47	24.32
12	1.138	25.52	83.62	24.29
13	1.138	25.43	83.84	24.26
14	1.137	25.11	83.97	23.98
15	1.139	25.58	83.68	24.38
16	1.135	25.72	82.51	24.08
17	1.143	25.47	83.39	24.28
18	1.142	25.68	83.42	24.47
19	1.141	25.82	83.34	24.56
20	1.139	25.75	83.69	24.54
21	1.136	25.57	80.88	23.50
22	1.136	25.46	80.88	23.38
23	1.135	25.37	80.37	23.14
24	1.134	25.13	80.40	22.91
25	1.133	25.25	80.16	22.93
26	1.132	25.07	79.82	22.65

27	1.138	25.79	83.42	24.49
28	1.137	25.82	83.86	24.62
29	1.138	25.77	83.41	24.45
30	1.125	26.08	80.88	23.74
31	1.125	26.01	80.53	23.56
32	1.124	26.01	80.21	23.44
33	1.123	25.89	80.21	23.31
34	1.119	25.92	80.28	23.28
35	1.114	25.86	80.82	23.28
36	1.114	25.74	80.99	23.23
37	1.115	25.65	80.89	23.13
38	1.115	25.51	80.69	22.95
39	1.114	25.43	79.98	22.66
40	1.105	25.88	80.45	23.02
41	1.106	25.73	80.84	23.00
42	1.106	25.72	80.50	22.90
43	1.106	25.56	80.53	22.77
44	1.106	25.47	80.07	22.56
45	1.104	25.55	79.14	22.33
46	1.105	25.44	79.48	22.34
47	1.105	25.31	79.46	22.22
48	1.105	25.18	79.60	22.14
49	1.107	25.73	79.69	22.70
50	1.106	25.58	79.95	22.63
51	1.107	25.44	80.04	22.53
52	1.106	25.33	79.59	22.30
53	1.106	25.32	79.44	22.25
54	1.105	25.19	79.30	22.08

55	1.087	26.22	79.17	22.56
56	1.091	25.74	80.33	22.56
57	1.093	25.75	80.30	22.60
58	1.096	25.69	80.66	22.72
59	1.096	25.63	80.59	22.64
60	1.098	25.54	80.37	22.53
Average	1.123±0.018	25.63±0.25	81.44±1.64	23.46±0.89

Table S6. PV parameters of 60 DFSA-treated devices.

Entry	V_{OC}(V)	J_{SC} (mAcm^{-2})	FF (%)	PCE (%)
1	1.137	25.80	84.15	24.70
2	1.135	25.72	83.87	24.48
3	1.134	25.84	83.83	24.56
4	1.132	25.79	83.61	24.42
5	1.131	25.79	83.56	24.38
6	1.130	25.80	83.40	24.32
7	1.137	25.93	82.99	24.45
8	1.135	25.87	83.34	24.48
9	1.135	25.82	83.46	24.45
10	1.133	25.77	83.42	24.35
11	1.132	25.71	83.56	24.31
12	1.130	25.72	83.31	24.22
13	1.147	25.90	83.65	24.86
14	1.147	25.91	83.75	24.88
15	1.146	25.84	83.58	24.76
16	1.146	25.88	83.53	24.77
17	1.145	25.84	83.70	24.77
18	1.153	25.99	83.30	24.95
19	1.151	25.86	83.38	24.81
20	1.150	25.84	83.23	24.72
21	1.149	25.88	83.29	24.76
22	1.147	25.87	83.04	24.65
23	1.149	25.89	83.35	24.79
24	1.148	25.79	83.42	24.70
25	1.148	25.83	83.23	24.67
26	1.147	25.74	83.29	24.59

27	1.152	25.99	84.36	25.25
28	1.151	25.94	84.17	25.14
29	1.150	25.87	84.24	25.07
30	1.156	25.92	84.33	25.25
31	1.155	25.87	84.29	25.20
32	1.155	25.79	84.41	25.14
33	1.154	25.77	84.24	25.05
34	1.155	25.90	84.33	25.22
35	1.155	25.77	84.32	25.09
36	1.154	25.76	84.38	25.08
37	1.153	25.69	84.59	25.06
38	1.153	25.70	84.33	24.98
39	1.150	25.27	86.03	25.00
40	1.156	25.92	84.33	25.25
41	1.155	25.87	84.29	25.20
42	1.155	25.79	84.41	25.14
43	1.154	25.77	84.24	25.05
44	1.155	25.90	84.33	25.22
45	1.155	25.77	84.32	25.09
46	1.154	25.76	84.38	25.08
47	1.153	25.69	84.59	25.06
48	1.153	25.70	84.33	24.98
49	1.147	25.46	82.30	24.04
50	1.146	25.47	82.27	24.02
51	1.146	25.41	82.23	23.94
52	1.145	25.39	82.25	23.91
53	1.134	25.49	82.96	23.98
54	1.133	25.36	83.03	23.87

55	1.123	26.03	80.34	23.48
56	1.126	26.04	80.91	23.73
57	1.127	26.03	80.70	23.67
58	1.126	25.80	80.88	23.49
59	1.125	25.82	80.57	23.40
60	1.124	25.73	80.48	23.27
Average	1.144±0.010	25.78±0.16	83.44±1.14	24.62±0.53

Table S7. PV parameters of 60 TFSA-treated devices.

Entry	V_{OC}(V)	J_{SC} (mAcm^{-2})	FF (%)	PCE (%)
1	1.169	26.07	84.61	25.78
2	1.169	26.07	85.06	25.92
3	1.166	25.87	84.43	25.47
4	1.165	25.90	84.20	25.40
5	1.163	25.79	83.98	25.19
6	1.163	25.80	84.30	25.29
7	1.162	25.73	83.85	25.07
8	1.165	25.58	84.58	25.21
9	1.162	25.65	84.14	25.09
10	1.163	26.13	84.08	25.55
11	1.157	25.96	83.65	25.13
12	1.156	25.96	83.79	25.14
13	1.158	25.76	83.93	25.05
14	1.157	25.77	83.95	25.04
15	1.158	26.06	83.80	25.29
16	1.158	26.05	84.00	25.34
17	1.157	26.05	83.82	25.28
18	1.156	26.09	83.75	25.26
19	1.150	26.09	83.74	25.13
20	1.152	25.91	83.86	25.02
21	1.153	26.11	84.35	25.39
22	1.152	25.99	84.36	25.25
23	1.151	25.94	84.17	25.14
24	1.150	25.87	84.24	25.07
25	1.150	25.27	86.03	25.00
26	1.156	26.06	84.26	25.38

27	1.156	25.92	84.33	25.25
28	1.155	25.87	84.29	25.20
29	1.155	25.79	84.41	25.14
30	1.154	25.77	84.24	25.05
31	1.151	26.09	83.69	25.12
32	1.155	25.90	84.33	25.22
33	1.155	25.77	84.32	25.09
34	1.154	25.76	84.38	25.08
35	1.153	25.69	84.59	25.06
36	1.163	26.07	85.02	25.77
37	1.157	25.92	84.44	25.34
38	1.157	25.87	84.20	25.20
39	1.155	25.81	84.10	25.08
40	1.158	25.81	83.80	25.05
41	1.155	25.85	83.74	25.01
42	1.154	25.88	83.73	25.00
43	1.157	25.94	83.01	24.93
44	1.158	25.88	84.02	25.18
45	1.157	25.80	84.03	25.09
46	1.155	25.88	84.20	25.18
47	1.155	25.97	84.20	25.25
48	1.154	26.06	84.24	25.33
49	1.153	26.05	84.20	25.28
50	1.157	26.07	84.28	25.41
51	1.156	26.01	84.34	25.35
52	1.154	25.96	84.14	25.21
53	1.153	25.90	84.08	25.11
54	1.152	25.90	84.00	25.07

55	1.154	26.08	84.07	25.30
56	1.153	26.03	84.04	25.22
57	1.152	26.01	83.73	25.09
58	1.151	26.01	83.78	25.09
59	1.156	25.97	83.74	25.15
60	1.168	25.77	85.28	25.66
Average	1.157±0.004	25.91±0.15	84.17±0.44	25.22±0.20

Table S8. The PV parameters for mini-modulate without and with TFSA treatment.

Minimodules	V_{OC} (V)	J_{SC} (mA cm^{-2})	FF (%)	PCE (%)
Control	6.52	4.10	76.07	20.34
TFSA	6.81	4.20	79.63	22.78

Table S9. EIS parameters of devices without and with SA-derivatives treatment.

Devices	Rtr (ohm)	CPE1 (F)	Rrec (ohm)	CPE2 (F)
Control	17121	1.08E-06	797230	1.90E-08
SA	16520	1.08E-08	822950	1.48E-08
DFSA	14932	1.10E-08	1005600	1.80E-08
TFSA	13959	1.01E-08	1215600	1.71E-08

Table S10. Time evolution of the PV parameters for PSCs without and with TFSA treatment.

	Time (h)	V_{OC} (V)	J_{SC} (mA cm^{-2})	FF (%)	PCE (%)
TFSA	0	1.17	26.07	85.06	25.92
	24	1.16	26.05	84.00	25.34

	48	1.15	25.91	83.86	25.02
	72	1.16	26.06	84.26	25.38
	264	1.15	25.96	83.73	25.01
	408	1.14	25.93	83.95	24.77
	624	1.13	25.85	83.98	24.61
	792	1.14	25.72	84.30	24.80
	936	1.13	25.95	83.89	24.65
	1080	1.13	25.81	82.97	24.21
	1464	1.14	25.87	84.40	24.88
	1848	1.12	26.08	83.27	24.27
	2064	1.11	25.83	82.75	23.77
	0	1.13	25.91	81.69	23.99
	24	1.13	25.72	81.43	23.67
	48	1.13	25.24	81.61	23.20
	72	1.13	25.30	82.50	23.56
	264	1.12	24.68	81.79	22.70
	408	1.12	24.92	81.58	22.73
Control	624	1.12	24.96	80.93	22.54
	792	1.12	24.92	80.55	22.39
	936	1.11	24.59	80.95	22.18
	1080	1.12	24.36	79.67	21.68
	1464	1.11	24.43	80.99	22.02
	1848	1.10	25.84	76.45	21.92
	2064	1.08	25.45	78.35	21.57

Table S11 Thermal aging of PSCs without and with TFSA treatment at 85 ºC hotplate.

Devices	Time (h)	V_{OC} (V)	J_{SC} (mA cm^{-2})	FF (%)	PCE (%)	Average PCE (%)	Standard deviation

		1.13	25.34	82.00	23.46		
	0	1.12	25.11	83.28	22.92	23.31	0.34
		1.13	25.37	82.07	23.55		
		1.09	25.37	83.76	23.17		
	24	1.07	24.81	80.42	21.32	22.16	0.94
		1.07	25.40	80.87	21.99		
		1.08	25.04	81.71	22.12		
	48	1.07	24.91	80.97	21.67	21.97	0.26
		1.07	25.61	80.92	22.12		
		1.06	25.80	79.79	21.87		
	72	1.05	25.86	77.99	21.20	21.31	0.51
		1.06	24.34	77.97	20.87		
		1.06	25.71	78.86	21.59		
	96	1.06	25.09	78.65	20.93	21.20	0.35
Control		1.05	25.43	79.19	21.08		
		1.05	25.61	77.41	20.74		
	144	1.05	25.33	77.41	20.60	20.40	0.47
		1.03	25.16	76.69	19.87		
		1.05	23.45	78.04	19.26		
	192	1.03	24.75	77.05	19.06	19.12	0.13
		1.05	23.16	78.41	19.03		
		1.03	24.39	76.87	19.39		
	216	1.04	23.33	76.39	18.52	19.09	0.49
		1.05	23.98	77.01	19.35		
		1.03	24.42	74.16	18.57		
	288	1.01	24.22	74.71	18.30	18.42	0.14
		1.03	23.92	74.75	18.39		
	336	1.01	24.12	73.75	17.99	17.68	0.39

		1.03	23.46	74.02	17.81		
		1.20	22.87	73.99	17.24		
		1.02	23.11	72.29	17.03		
	432	1.03	23.38	67.79	16.26	16.79	0.46
		1.03	22.74	73.24	17.07		
		1.00	22.72	70.81	16.10		
	504	1.01	21.85	72.30	15.90	15.72	0.50
		1.00	21.98	69.14	15.16		
		1.00	22.57	68.85	15.56		
	552	1.00	21.00	66,55	14.04	14.75	0.76
		1.02	20.42	70.20	14.65		
		1.01	21.53	67.81	14.75		
	600	0.99	20.32	65.45	13.29	13.84	0.79
		1.00	21.59	61.99	13.49		
		1.14	26.06	84.69	25.19		
	0.00	1.15	25.82	84.29	25.11	25.16	0.04
		1.15	26.01	83.89	25.18		
		1.11	26.27	83.89	24.55		
	24.00	1.11	25.84	83.30	23.85	23.88	0.66
		1.10	25.49	83.17	23.23		
		1.10	26.18	83.52	24.03		
TFSA	48.00	1.09	26.10	82.05	23.37	23.49	0.49
		1.09	25.78	81.96	23.08		
		1.08	26.11	81.99	23.21		
	72.00	1.09	25.57	81.08	22.63	22.91	0.29
		1.07	25.80	82.72	22.89		
		1.08	25.83	80.04	22.38		
	96.00	1.09	25.82	80.04	22.38	22.33	0.09

	1.07	25.96	79.66	22.22		
	1.05	25.33	77.41	20.60		
144.00	1.06	24.42	77.62	20.05	20.40	0.30
	1.05	25.03	78.44	20.55		
	1.06	25.32	78.78	21.13		
192.00	1.05	25.17	78.76	20.87	20.92	0.19
	1.05	25.17	78.31	20.77		
	1.04	24.63	77.94	20.07		
216.00	1.05	24.39	78.54	20.12	20.14	0.09
	1.05	24.59	78.27	20.24		
	1.05	24.54	77.77	20.10		
288.00	1.05	24.36	77.69	19.77	19.88	0.19
	1.05	24.28	77.84	19.76		
	1.03	24.33	76.91	19.28		
336.00	1.05	24.46	75.15	19.26	19.32	0.08
	1.06	24.33	75.03	19.41		
	1.03	22.21	81.37	18.64		
432.00	1.02	24.10	74.48	18.36	18.37	0.26
	1.02	23.61	75.03	18.12		
	1.02	22.27	79.20	18.09		
504.00	1.03	23.66	74.27	18.15	18.11	0.03
	1.03	22.27	79.20	18.09		
	1.04	23.80	75.21	18.77		
552.00	1.03	23.29	74.00	17.75	18.50	0.66
	1.03	23.70	77.62	18.98		
	1.05	23.30	74.94	18.36		
600.00	1.03	23.38	75.89	18.22	18.45	0.28
	1.05	23.75	75.06	18.76		

References

1. C. Luo, G. Zheng, F. Gao, X. Wang, C. Zhan, X. Gao and Q. Zhao, *Nat. Photonics*, 2023, **17**, 856-864.
2. W.-Q. Wu, P. N. Rudd, Z. Ni, C. H. Van Brackle, H. Wei, Q. Wang, B. R. Ecker, Y. Gao and J. Huang, *J. Am. Chem. Soc.*, 2020, **142**, 3989-3996.
3. S. Chen, Y. Liu, X. Xiao, Z. Yu, Y. Deng, X. Dai, Z. Ni and J. Huang, *Joule*, 2020, **4**, 2661-2674.
4. B. Gao and J. Meng, *Appl. Surf. Sci.*, 2020, **530**, 147240.
5. K. M. Reza, A. Gurung, B. Bahrami, A. H. Chowdhury, N. Ghimire, R. Pathak, S. I. Rahman, M. A. R. Laskar, K. Chen, R. S. Bobba, B. S. Lamsal, L. K. Biswas, Y. Zhou, B. Logue and Q. Qiao, *Sol. RRL*, 2021, **5**, 2000740.
6. G. Xu, R. Xue, S. J. Stuard, H. Ade, C. Zhang, J. Yao, Y. Li and Y. Li, *Adv. Mater.*, 2021, **33**, 2006753.
7. Q. Jiang, J. Tong, Y. Xian, R. A. Kerner, S. P. Dunfield, C. Xiao, R. A. Scheidt, D. Kuciauskas, X. Wang, M. P. Hautzinger, R. Tirawat, M. C. Beard, D. P. Fenning, J. J. Berry, B. W. Larson, Y. Yan and K. Zhu, *Nature*, 2022, **611**, 278-283.
8. Y. Zhang, R. Yu, M. Li, Z. He, Y. Dong, Z. Xu, R. Wang, Z. Ma and Z. Tan, *Adv. Mater.*, 2024, **36**, 2310203.
9. Z.-R. Lan, Y.-D. Wang, J.-Y. Shao, D.-X. Ma, Z. Liu, D. Li, Y. Hou, J. Yao and Y.-W. Zhong, *Adv. Funct. Mater.*, 2024, **34**, 2312426.
10. P. Chen, Y. Xiao, J. Hu, S. Li, D. Luo, R. Su, P. Caprioglio, P. Kaienburg, X. Jia, N. Chen, J. Wu, Y. Sui, P. Tang, H. Yan, T. Huang, M. Yu, Q. Li, L. Zhao, C.-H. Hou, Y.-W. You, J.-J. Shyue, D. Wang, X. Li, Q. Zhao, Q. Gong, Z.-H. Lu, H. J. Snaith and R. Zhu, *Nature*, 2024, **625**, 516-522.
11. Q. Jiang, R. Tirawat, R. A. Kerner, E. A. Gaulding, Y. Xian, X. Wang, J. M. Newkirk, Y. Yan, J. J. Berry and K. Zhu, *Nature*, 2023, **623**, 313-318.
12. B. Zhou, C. Shang, C. Wang, D. Qu, J. Qiao, X. Zhang, W. Zhao, R. Han, S. Dong, Y. Xue, Y. Ke, F. Ye, X. Yang, Y. Tu and W. Huang, *Research*, 2024, **7**, 0309.

13. Z. He, M. Li, H. Jia, R. Yu, Y. Zhang, R. Wang, Y. Dong, X. Liu, D. Xu and Z. a. Tan, *Adv. Mater.*, 2023, **35**, 2304918.